symmetry

MDPI

Article

Spatial Cognitive Electroencephalogram Network Topological Features Extraction Based on Cross Fuzzy Entropy Network Graph

Yanhong Zhou [1,†], Xulong Liu [2,†], Dong Wen [3], Shuang Xu [2], Xianglong Wan [3] and Huibin Lu [1,*]

[1] School of Information Science and Engineering, Yanshan University, Qinhuangdao 066004, China; xjwd@ysu.edu.cn
[2] School of Computer and Communication Engineering, Northeastern University, Qinhuangdao 066004, China; liuxulong@neuq.edu.cn (X.L.); 2272179@stu.neu.edu.cn (S.X.)
[3] School of Intelligence Science and Technology, University of Science and Technology Beijing, Beijing 100083, China; aiwd168@ustb.edu.cn (D.W.); wanxianglong@ustb.edu.cn (X.W.)
* Correspondence: hblu168@163.com; Tel.: +86-3358618609
† These authors contributed equally to this paper.

Abstract: Spatial cognition, a critical component of human cognitive function, can be enhanced through targeted training, such as virtual reality (VR)-based interventions. Recent advances in electroencephalography (EEG)-based functional connectivity analysis have highlighted the importance of network topology features for understanding cognitive processes. In this paper, a framework based on a cross fuzzy entropy network graph (CFENG) is proposed to extract spatial cognitive EEG network topological features. This framework involves calculating the similarity and symmetry between EEG channels using cross fuzzy entropy, constructing weighted directed network graphs, transforming one-dimensional EEG signals into two-dimensional brain functional connectivity networks, and extracting both local and global topological features. The model's performance is evaluated and interpreted using an XGBoost classifier. Experiments on an EEG dataset from group spatial cognitive training validated the CFENG model. In the Gamma band, the CFENG achieved 97.82% classification accuracy, outperforming existing methods. Notably, the asymmetrically distributed EEG channels Fp1, P8, and Cz contributed most to spatial cognitive signal classification. An analysis after 28 days of training revealed that specific VR games enhanced functional centrality in spatial cognition-related brain regions, reduced information flow path length, and altered information flow symmetry. These findings support the feasibility of VR-based spatial cognitive training from a brain functional connectivity perspective.

Keywords: spatial cognition; electroencephalogram; network feature extraction; cross fuzzy entropy network graph

check for updates

Academic Editor: Alice Miller

Received: 6 November 2024
Revised: 30 January 2025
Accepted: 1 February 2025
Published: 6 February 2025

Citation: Zhou, Y.; Liu, X.; Wen, D.; Xu, S.; Wan, X.; Lu, H. Spatial Cognitive Electroencephalogram Network Topological Features Extraction Based on Cross Fuzzy Entropy Network Graph. *Symmetry* **2025**, *17*, 243. https://doi.org/10.3390/sym17020243

Copyright: © 2025 by the authors. Licensee MDPI, Basel, Switzerland. This article is an open access article distributed under the terms and conditions of the Creative Commons Attribution (CC BY) license (https://creativecommons.org/licenses/by/4.0/).

1. Introduction

Spatial cognition represents a complex cognitive function encompassing various abilities, including spatial observation, spatial memory, spatial imagination, and spatial reasoning [1]. This cognitive domain is essential for the encoding of information pertaining to the environment, spatial orientation, and spatial relationships, which are manifested in both short-term and long-term working memory [2]. Research indicates that as individuals age, their spatial cognitive abilities tend to decline, resulting in varying degrees of deterioration in spatial memory, visuospatial structuring, and orientation among the

elderly population. Empirical studies have demonstrated that spatial cognitive abilities are amenable to training. Specifically, individuals exhibiting diminished spatial cognitive skills can experience improvements through targeted spatial cognitive training interventions [1,3]. Consequently, the implementation and assessment of spatial cognitive training hold significant implications for the diagnosis and rehabilitation of patients with mild cognitive impairment (MCI) who present with spatial orientation difficulties [4].

Addressing the limitation of traditional spatial cognitive training and evaluation methods, which tend to be monolithic, existing research has explored the utilization of VR and brain–computer interfaces (BCIs) to devise a multifaceted spatial cognitive training and evaluation system that fosters greater participant engagement. Kuliga et al. [5] demonstrated that there is no discernible difference in the manner by which humans perceive routes in virtual environments compared to real-world settings. White et al. [6] conceived a VR-based spatial navigation training program, which, upon implementation, led to a marked improvement in the navigational abilities of Alzheimer's patients. Cardenas-Delgado et al. [7] introduced a Virtual Maze Task (VMT) grounded in VR and experimentally validated its efficacy in assessing short-term memory and spatial memory. Wen et al. [1,8,9] further contributed by developing a BCI-VR-integrated spatial cognition training and evaluation system. This system employed tasks such as VR water maze, virtual car navigation, virtual city street exploration, and virtual farm management to train users' spatial cognition and achieved promising outcomes [10].

To effectively evaluate the effectiveness of VR game-based spatial cognition training, EEG signals are considered a powerful tool. Relevant studies [1] indicate that changes in spatial cognition abilities following VR game training result in corresponding modifications in EEG patterns related to spatial cognition. This is evidenced by EEG data, which demonstrate that the signals before and after spatial cognition training are distinguishable and classifiable. Qiu and Lin et al. have established a correlation between EEG signals and spatial cognitive ability, rendering EEG signal classification a prevalent tool for such assessments [11,12]. In recent years, numerous machine learning techniques have been employed to analyze EEG signals pertaining to spatial cognitive ability, including independent component analysis (ICA) [13,14], spectral analysis [13,15,16], and event-related potential analysis [14,17–19]. These methodologies primarily analyze spatially cognitive EEG signals from temporal or frequency domains. Recently, spatial cognition EEG signal classification methods based on functional connectivity and spatial features have emerged. Wen et al. [1] developed a home-based Spatial Cognitive Training and Evaluation System, integrating VR and EEG to train subjects for 20 days and analyze brain activity changes. Results revealed significant behavioral improvements and Granger causality analysis (GCA) differences across EEG frequency bands after four days, highlighting the system's potential for spatial cognitive assessment and rehabilitation. Yan et al. [20] investigated depressive emotion-related spatial cognition impairment using an EEG-based network analysis. Functional connectivity networks were constructed based on the phase- locking value (PLV), with EEG electrodes as nodes and PLV values as edges. Results revealed stronger left frontoparietal network connections in Delta, Beta, and Gamma bands during spatial tasks, suggesting compensatory brain reorganization. Dong et al. [8] proposed a feature extraction technique for EEG signals based on a mutual information co-space mode of arrangement conditions (PCMICSPs), utilizing a CNN for binary classification of EEG signals before and after VR spatial cognitive training, achieving an average classification accuracy of 98%. Wen et al. [10] further contributed by presenting a multi-spectral image transformation feature of multi-dimensional conditional mutual information (MCMI) and employed a CNN model to classify EEG signals before and after VR game training. Across all band

combinations, the Beta1–Beta2–Gamma combination exhibited the highest classification accuracy, reaching 98%.

The aforementioned research presents three primary issues: (1) Given the complexity of spatial cognitive EEG patterns, the extraction of network topological features from the perspective of brain functional connectivity may be more effective for decoding spatial cognitive EEG signals than traditional temporal, frequency, or spatial features. However, existing studies on spatial cognitive EEG signals have not addressed the brain network level. (2) While prior research has examined the classification performance of various combinations of EEG frequency bands, there is a lack of detailed analysis focused on specific single frequency bands. (3) Current studies have not explored the interpretability of the proposed classification models, particularly the analysis of the importance of different brain electrical channels for spatial cognition. To address these three issues, this paper proposes a method for extracting network topology features for a spatial cognitive EEG classification model, emphasizing the interpretability of single-band non-linear feature cross fuzzy entropy network graphs. Building on findings from previous studies [1,8,9] that indicate the statistical dependence of time series signals across different EEG channels is relevant for spatial cognitive EEG classification, we employed cross fuzzy entropy as a non-linear feature to analyze interactions between different EEG channels. This approach facilitated the construction of EEG functional connectivity networks and the extraction of single-band network topological features, thereby enhancing the interpretability of the spatial cognitive EEG signal classification model.

Therefore, the purpose of this paper is to address the aforementioned issues in the following aspects: (1) A topological feature extraction method of functional connection network of spatial cognitive EEG based on a cross fuzzy entropy network graph is proposed. (2) The effects of different frequency bands (Delta, Theta, Alpha1, Alpha2, Beta1, Beta2, and Gamma) on the classification of spatial cognitive EEG are discussed. (3) Based on functional connectivity networks from electroencephalography (EEG), the importance of different channels for spatial cognitive EEG classification was analyzed, with the aim of enhancing the interpretability of the model.

2. Methods

The overall methodology of the proposed approach is illustrated in Figure 1. Initially, EEG signals are collected both prior to and following spatial cognitive training. These signals undergo preprocessing to eliminate noise and are subsequently segmented into a series of independent epochs, thereby forming a comprehensive dataset. Following this, feature extraction is performed, which encompasses three components: the calculation of cross fuzzy entropy between two EEG channels, the computation of the adjacency matrix, and the extraction of topological features from the EEG functional connectivity network. Ultimately, the XGBoost algorithm is employed to classify the spatial cognitive EEG signals and to elucidate the model. A detailed explanation of these processes is provided in the subsequent sections.

2.1. Dataset

1. Basic Information of the Subject

In Beijing University of Science and Technology (USTB), 16 male subjects were recruited to participate in the group spatial cognitive training experiment. The subjects were 20–27 years old, with normal vision, and had no prior history of mental illness or similar experiment experience. All subjects gave their informed consent for inclusion before they participated in the study. The study was conducted in accordance with the Declaration of Helsinki, and the protocol was approved by the Ethics Committee of University of

Science and Technology Beijing (Project identification code is No. 2022-1-104, and the date of approval is 4 March 2022).

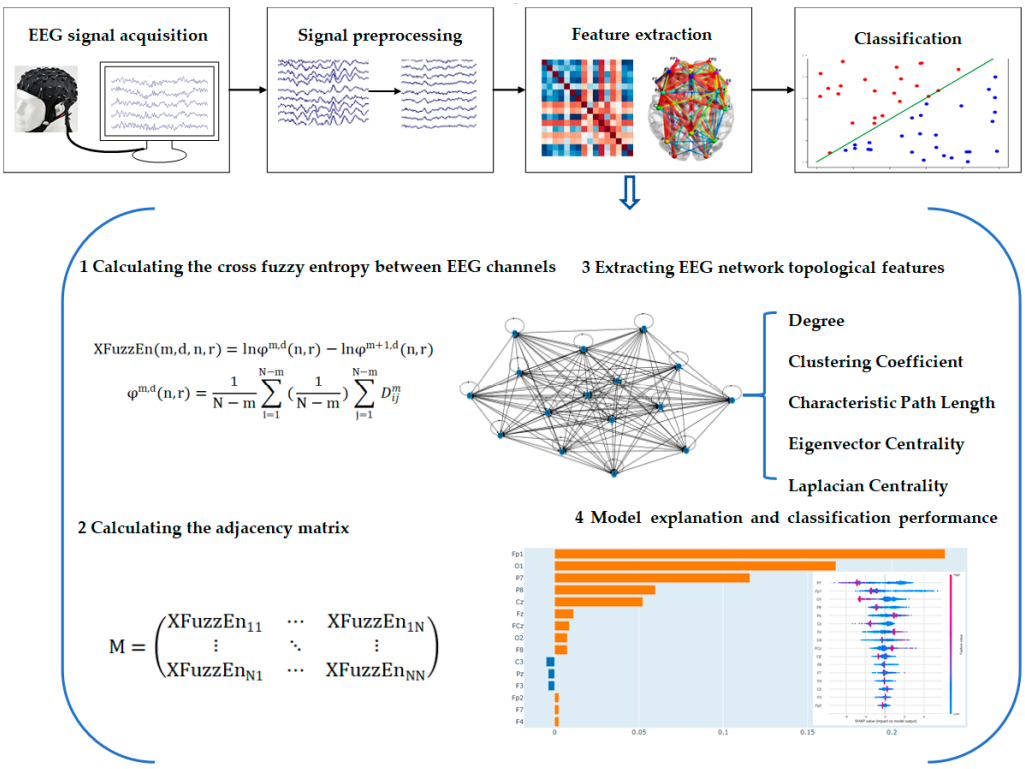

Figure 1. General process of feature extraction and classification of spatial cognitive EEG networks.

2. Experimental Scheme of Group Spatial Cognitive Training

The 16 subjects were divided into 4 groups, with 4 people in each group divided into 2 teams and 2 people in each team, and underwent group spatial cognition training for 28 days. The training was based on VR racing games, subspatial coding and decoding. Subjects first memorized the training route (encoding) and then repeated the path (decoding). After 28 days, the spatial cognitive ability was tested, including the test game and three assessment scales. The Test the Virtual City Walking (VCW) game was conducted by memorizing the path and then roaming to the end. EEG and behavioral data were recorded during training and testing to assess spatial cognitive ability. Figures 2 and 3 show the training and test game scenarios, respectively. The VR device uses the HTC Vive Pro with a resolution of 2880×1600 and a refresh rate of 90 Hz.



Figure 2. Typical task pathways and game scenarios in spatial cognitive training.

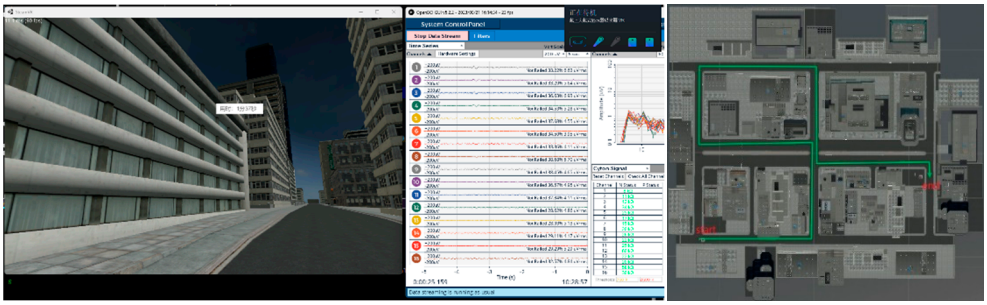

Figure 3. Experimental framework and standardized task sequence for spatial cognition assessment.

3. Acquisition and Preprocessing of Electroencephalogram (EEG) Data

To assess the spatial cognitive abilities of the experimental subjects, it is essential to collect EEG signals from each participant during the spatial cognitive test. In this study, an OpenBCI EEG device equipped with 16 wet electrodes was utilized for EEG data acquisition, with electrode placements configured according to the international 10–20 system. The EEG channels recorded in this investigation include Fp1, Fp2, F7, F3, Fz, F4, F8, FCz, C3, C4, Cz, P3, P4, Pz, O1, and O2, totaling 16 channels. Reference electrodes A1 and A2 were positioned at the vertical mastoids of both ears. The arrangement of EEG electrodes employed in this study is illustrated in Figure 4. Brain networks often exhibit small-world properties, which are relatively stable to minor perturbations in electrode placement. In this study, careful attention to electrode placement and rigorous quality control, combined with methodological approaches to normalize and validate connectivity measures, further mitigates the impact of these variations and enhances the reliability of network topology analysis in EEG studies.

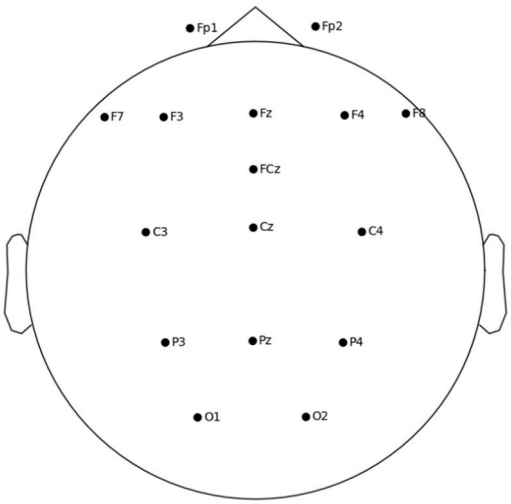

Figure 4. Distribution of EEG electrodes.

During the experiment, the EEG signals were sampled at a frequency of 500 Hz and preprocessed using the EEGLAB toolbox [21]. Initially, the raw EEG signals were imported into the EEGLAB toolbox, followed by the selection of specific electrode channels: Fp1, Fp2, F7, F3, Fz, F4, F8, FCz, C3, C4, Cz, P3, P4, Pz, O1, and O2, which were utilized for electrode positioning in this study. The imported EEG signals were then subjected to a notch filter to eliminate 50 Hz power frequency interference and a bandpass filter ranging from 1 to 50 Hz to remove high-frequency noise and low-frequency drift. Baseline correction and the removal of poor-quality data were also conducted to ensure the quality of the EEG signals. Subsequently, ICA was employed to remove noise components from the EEG

signals, primarily including eye movements and myoelectric artifacts. Finally, the EEG signal was divided into seven frequency bands using bandpass filters: Delta (1.0–4.0 Hz), Theta (4.0–8.0 Hz), Alpha1 (8.0–10.5 Hz), Alpha2 (10.5–13.0 Hz), Beta1 (13.0–20.0 Hz), Beta2 (20.0–30.0 Hz), and Gamma (30.0–40.0 Hz).

In this study, a traceable time window method was employed to extract EEG signals in epochs, as described in [9]. Initially, the event marker was identified from the inception of the EEG signal. Upon locating an event marker, the signals encompassing 1 s before and 1 s after the marker were designated as epochs. The search for subsequent event markers then proceeded in a backward direction. If the 1-s time window preceding and following the next marker overlapped with the preceding epoch, the two epochs were amalgamated; otherwise, they were extracted as distinct epochs. After collecting and amalgamating meaningful epochs as delineated above, a sliding window technique was utilized to segment the EEG signals, with a window size of 2 s and an overlap rate of 50%. Consequently, due to the disparity in the durations of the two test tasks administered before and after training, the EEG signals from each frequency band were ultimately segmented into 1380 and 1294 samples, respectively. To reduce the computational burden during cross fuzzy entropy calculation, we followed established practices and downsampled the data to 125 Hz after dividing the EEG signal into specific frequency bands and segmenting them into epochs.

2.2. Method for Extracting Network Features of Spatial Cognitive Electroencephalogram (EEG) Based on the Cross Fuzzy Entropy Network Graph

In this study, we treated each EEG channel as a distinct node within a functionally connected network. The cross fuzzy entropy between two channels was calculated and utilized as the weight of the edge connecting the two nodes. By traversing the weights of all edges, an adjacency matrix was formed, which was then used to generate a weighted directed network graph. From this graph, network topological features were extracted.

1. Cross Fuzzy Entropy

Fuzzy entropy essentially measures the probability of generating a new pattern as the dimension of a time series change. The higher the probability of a sequence generating a new pattern, the greater the complexity of the sequence and the higher its entropy [22,23]. Cross fuzzy entropy is an extension of fuzzy entropy and is capable of measuring the synchronization or similarity between time series. The more synchronous two time series are, the smaller the value of their cross fuzzy entropy [24]. The specific algorithm for calculating cross fuzzy entropy is detailed as follows:

(1) Sequence Segmentation: For two time series $\{t(i), 1 \le i \le N\}$ and $\{s(i), 1 \le j \le N\}$, given embedding dimension m and delay d, N-m vector sequences $\{t(i), t(i+d), \cdots, t(i+(m-1)d), 1 \le i \le N-m\}$ and $\{s(j), s(j+d), \cdots, s(j+(m-1)d), 1 \le j \le N-m$ are constructed, and vector templates $X_{i,d}^{m}$ and $Y_{j,d}^{m}$ are defined as follows:

$$X_{i,d}^{m} = \{u(i), u(i+d), \cdots, u(i+(m-1)d)\} - \overline{u}(i) \quad (1)$$

$$Y_{j,d}^{m} = \{v(j), v(j+d), \cdots, v(j+(m-1)d)\} - \overline{v}(j) \quad (2)$$

among

$$\overline{u}(i) = \frac{1}{m}\sum_{l=0}^{m-1} u(i+ld) \quad (3)$$

$$\overline{v}(j) = \frac{1}{m}\sum_{l=0}^{m-1} v(j+ld) \quad (4)$$

(2) Calculating Distance: Define the distance between vector template $X_{i,d}^{m}$ and $Y_{j,d}^{m}$ as Chebyshev distance, that is, the maximum value of the absolute difference of the values of each element in the corresponding position in the two vectors, as follows:

$$d_{ij}^{m} = [X_{i,d}^{m}, Y_{j,d}^{m}] = \max_{k\in(0,m-1)} |u(i+kd) - \overline{u}(i) - (v(j+kd) - \overline{v}(j))| \quad (5)$$

(3) Define Similarity: The synchronization or similarity D_{ij}^{m} between $X_{i,d}^{m}$ and $Y_{j,d}^{m}$ is calculated by the fuzzy function $\mu(d_{ij}^{m}, n, r)$ as follows:

$$D_{ij}^{m} = \mu(d_{ij}^{m}, n, r) \quad (6)$$

where, the fuzzy function $\mu(d_{ij}^{m}, n, r)$ is an exponential function

$$\mu(d_{ij}^{m}, n, r) = \exp\left[-\frac{\left(d_{ij}^{m}\right)^{n}}{r}\right] \quad (7)$$

In the formula, r and n are the width and gradient of the boundary of the exponential function, respectively. According to the suggestion of previous research [25], r and n are set as 0.2 and 2, respectively.

(4) Define the Repeat Probability Function of the Same Pattern:

$$\varphi^{m,d}(n, r) = \frac{1}{N-m}\sum_{i=1}^{N-m}\left(\frac{1}{N-m}\right)\sum_{j=1}^{N-m} D_{ij}^{m} \quad (8)$$

Then, extend the embedding dimension m to m + 1, repeat the above steps to calculate the distance d_{ij}^{m+1} between $X_{i,d}^{m+1}$ and $Y_{j,d}^{m+1}$, and calculate the similarity $\varphi^{m+1,d}(n, r)$.

(5) Define the Cross Fuzzy Entropy (XFuzzEn) as follows:

$$XFuzzEn(m, d, n, r) = \ln\varphi^{m,d}(n, r) - \ln\varphi^{m+1,d}(n, r) \quad (9)$$

The cross fuzzy entropy is a powerful tool for quantifying the synchrony between two time series, particularly in complex systems like brain networks. Its robustness to noise and ability to capture non-linear dependencies make it well-suited for analyzing EEG signals in spatial cognition studies. However, its reliance on parameter tuning and computational complexity are potential limitations that need to be addressed in practical applications.

2. Adjacency Matrix

In this approach, N EEG channels are taken as nodes in the EEG functional connection network. The cross fuzzy entropy between any two EEG signals from these channels is utilized as the weight of the connecting edges between the corresponding nodes. Subsequently, the adjacency matrix M is computed based on these weights as follows:

$$M = \begin{pmatrix} XFuzzEn_{11} & \cdots & XFuzzEn_{1N} \\ \vdots & \ddots & \vdots \\ XFuzzEn_{N1} & \cdots & XFuzzEn_{NN} \end{pmatrix} \quad (10)$$

where XFuzzEnij is the cross fuzzy entropy between EEG channel i and EEG channel j.

3. Network Topology Features

Network topological features were used to calculate functional connectivity patterns in EEG data induced by spatial cognitive tasks. Based on graph theory, topological features

are divided into global features and local features [26]. The global characteristics used in this study include characteristic path length (PL) and clustering coefficient (CC). Local features include degree, eigenvector centrality (EC), and Laplacian centrality (LPC).

(1) Degree

The degree serves as the most direct metric for assessing the centrality of nodes within a network in the context of graph theory. In the EEG functional connectivity network, each node corresponds to a channel. A higher degree of a node indicates a stronger connection with other channels, thereby reflecting increased centrality and activity of that channel, which signifies its greater importance within the network. In a weighted graph, the degree of a node is quantified as the sum of the weights of the edges that are adjacent to the node, as follows:

$$\deg(u) = \sum_{u,v \in V} \omega_{uv} \tag{11}$$

(2) Characteristic Path Length

The characteristic path length [27] is defined as the arithmetic average of the shortest path length between all potential node pairs in the network, namely:

$$a = \sum_{s,t \in V, s \neq t} \frac{d(s,t)}{n(n-1)} \tag{12}$$

where V is the set of nodes in graph G, d(s, t) is the shortest path from node s to node t, and n is the number of nodes in graph G.

As an indicator to evaluate the functional integration of brain regions, the characteristic path length reflects the efficiency of global communication of EEG. The lower the feature path length is, the closer the functional integration between brain regions is and the smoother the information transmission between brain regions is.

(3) Clustering Coefficient

Clustering coefficients are extensively utilized to assess the degree of functional segregation among brain regions, offering significant information into the efficiency of local neural networks. Specifically, the clustering coefficient quantifies the extent to which adjacent nodes within a given brain region are interconnected in a neural network. A higher clustering coefficient signifies a greater frequency and strength of interactions among neighboring nodes within that brain region, suggesting that the region exhibits a more cohesive functional connectivity and enhanced efficiency.

In the context of a weighted graph, the clustering coefficient of a node u is defined as the geometric mean value of any two nodes v forming a triangle with node u and the edge weights among them [28,29], as follows:

$$c_u = \frac{1}{\deg(u)(\deg(u)-1)} \sum_{v\omega} (\hat{\omega}_{uv} \hat{\omega}_{u\omega} \hat{\omega}_{v\omega})^{1/3} \tag{13}$$

where $\deg(u)$ is the degree of node u. The edge weight $\hat{\omega}_{uv}$ is normalized according to the maximum weight in the network, namely:

$$\hat{\omega}_{uv} = \omega_{uv} / \max(\omega) \tag{14}$$

(4) Eigenvector Centrality

Eigenvector centrality [27] serves as a metric for assessing the significance of nodes within a network. This measure evaluates the centrality of nodes by considering both the connectivity among nodes and the importance of the connected entities. It is particularly

effective for identifying genuine "influencers" or pivotal nodes within a network. The value range of eigenvector centrality is [0, 1], and the greater the value, the greater the centrality.

The eigenvector centrality of a node in the graph G is computed iteratively by the centrality of its previous node. The centrality of node i is the i-th element of the eigenvector associated with the principal eigenvalue λ. The eigenvector x is defined by the following equation, where the eigenvalue with the largest absolute value is called the principal eigenvalue, as follows:

$$\lambda xT = xTA \tag{15}$$

where A is the adjacency matrix of graph G. By defining the row-column product, the above equation is equivalent to

$$\lambda x_i = \sum_{j \to i} x_j \tag{16}$$

The eigenvector centrality of node i is obtained by adding the eigenvector centralities of the nodes preceding node i and dividing by λ.

(5) Laplacian Centrality

Laplacian centrality [30] serves as an indicator of a node's significance within a network, providing insights into the actual influence and relevance of nodes. The Laplacian centrality of a node i is quantified by the reduction in Laplacian energy that occurs upon the removal of node i from the graph. Specifically, Laplacian energy is defined as the summation of the squares of the eigenvalues of the graph's Laplacian matrix, as follows:

$$C_L(u_i, G) = \frac{(\Delta E)_i}{E_L(G)} = \frac{E_L(G) - E_L(G_i)}{E_L(G)} \tag{17}$$

$$E_L(G) = \sum_{i=0}^{n} \gamma_i^2 \tag{18}$$

where $E_L(G)$ is the Laplacian energy of graph G, $E_L(G_i)$ is the Laplacian energy of graph G after removing node i, and γ_i is the eigenvalue of the Laplacian matrix of graph G.

2.3. Classifier and Evaluation Index

In this study, we constructed an XGBoost (Extreme Gradient Boosting) model to classify spatial cognitive EEG signals. XGBoost is an ensemble learning algorithm rooted in the Gradient Boosting Decision Tree (GBDT) framework [31]. The fundamental principle of XGBoost involves integrating multiple weak classifiers (decision trees) into a robust classifier. This process entails training each decision tree based on the residuals from the preceding tree, iteratively optimizing the loss function to progressively minimize these residuals. Additionally, the model mitigates the risk of overfitting by meticulously controlling the complexity and incorporating regularization terms of the trees. Furthermore, XGBoost enhances GBDT through several key innovations, including the utilization of second-order Taylor approximations of loss functions to expedite the optimization process, the introduction of regularization terms to bolster model stability, the implementation of parallel computations to elevate training efficiency, and the design of proficient strategies for processing missing values. These advancements collectively contribute to substantial improvements in model performance and generalization capabilities.

In this paper, the input features for the XGBoost model are derived from the topological characteristics of the functional connection network of EEG signals. The output of the model is the classification of spatial cognitive EEG signals, comparing EEG signals recorded during the pre-training test session and the post-training test session. To evaluate the efficacy of XGBoost, we conducted a comparative analysis with various other classifiers, including Random Forests (RFs), Gradient Boosting Classifiers (GBCs), AdaBoost Classifiers (Adas), Decision Trees (DTs), Multi-Layer Perceptrons (MLPs), K-Nearest Neighbors (KNNs),

Linear Discriminant Analysis (LDA), and Support Vector Machines (SVMs). To assess the generalization error associated with different topological features in spatial cognitive EEG classification, we followed the methodology outlined by Wen et al. [1,8,9]. EEG data from all 16 participants were used, with each participant contributing multiple epochs (time segments). For instance, EEG signals from each frequency band were segmented into 1380 pre-training and 1294 post-training samples, resulting in a total dataset of 2674 samples. This large number of epochs ensured sufficient data for training and evaluating the binary classifier. To enhance the robustness of the results and address the risk of overfitting, a five-repeated nested cross-validation strategy was adopted. In this approach, the inner loop utilized 10-fold cross-validation for model training and hyperparameter optimization, while the outer loop employed 5-fold cross-validation to evaluate the model's generalization performance. As a result, each model underwent a total of 25 evaluations.

In the context of spatial cognitive EEG classification, the outcomes can be categorized into four types based on the combination of the true category and the output of the XGBoost classifier: True Positives (TPs), False Positives (FPs), True Negatives (TNs), and False Negatives (FNs).

The evaluation of the generalization performance of the XGBoost classifier is conducted using a confusion matrix, which incorporates five key metrics: accuracy, recall, precision, F1 score, and Area Under the Curve (AUC). The formulas for calculating these metrics are as follows:

$$\text{Accuracy} = (\text{TP} + \text{TN})/(\text{TP} + \text{TN} + \text{FP} + \text{FN}) \tag{19}$$

$$\text{Precision} = \text{TP}/(\text{FP} + \text{TP}) \tag{20}$$

$$\text{Recall} = \text{TP}/(\text{TP} + \text{FN}) \tag{21}$$

$$\text{F1 score} = 2 \times \text{Precision} \times \text{Recall}/(\text{Precision} + \text{Recall}) \tag{22}$$

The Area Under the Curve (AUC) represents the area of the Receiver Operating Characteristic (ROC) curve, with the horizontal axis corresponding to the false positive rate (FPR). The vertical coordinate of the ROC curve is calculated in the same manner as Recall. The FPR indicates the proportion of actual negative samples that are incorrectly predicted as positive. A larger AUC signifies a greater area under the curve, and a curve that bulges more towards the upper left corner indicates superior model performance.

3. Results

In order to assess the validity of the proposed topological features of functionally-connected networks derived from EEG for the classification of spatial cognitive EEG signals, this section presents experimental results that compare various network topological features with alternative methodologies. These include three deep learning models and two classical feature extraction models. Furthermore, this section discusses the classification performance of different EEG functional connectivity networks, examines the parameter selection process for these networks, and analyzes the significance of various channels in the classification of spatial cognitive EEG signals.

3.1. Comparative Analysis of Topological Feature Classification Performance Across Various Electroencephalogram (EEG) Functional Connectivity Networks

In this study, we systematically evaluate the classification performance of five representative network topological features across seven distinct frequency bands. The analysis, as presented in Tables 1–3, reveals a clear hierarchy in classification efficacy across the frequency band. The bands are ranked in descending order of performance as follows:

Gamma band, Beta2 band, Beta1 band, Delta band, Theta band, Alpha1 band, and Alpha2 band. Notably, the Gamma band consistently demonstrates superior classification performance, with all evaluation metrics—including Accuracy, AUC, and F1 score—significantly outperforming those of other frequency bands.

Table 1. Comparative analysis of classification accuracy for various network topological features across multiple frequency bands.

Feature	Frequency Band						
	Delta	**Theta**	**Alpha1**	**Alpha2**	**Beta1**	**Beta2**	**Gamma**
Degree	0.8810	0.8657	0.8557	0.8500	0.9294	0.9687	0.9782
PL	0.7429	0.7205	0.7093	0.6862	0.7322	0.8097	0.8359
EC	0.8578	0.8434	0.8215	0.7852	0.9134	0.9594	0.9711
CC	0.8332	0.8049	0.7536	0.7419	0.8568	0.9316	0.9407
LPC	0.8589	0.8434	0.8210	0.7830	0.9097	0.9604	0.9759

Table 2. Comparative analysis of AUC values for various network topological features across multiple frequency bands.

Feature	Frequency Band						
	Delta	**Theta**	**Alpha1**	**Alpha2**	**Beta1**	**Beta2**	**Gamma**
Degree	0.9523	0.9422	0.9303	0.9288	0.9800	0.9928	0.9965
PL	0.7897	0.7806	0.7644	0.7510	0.7954	0.8515	0.8813
EC	0.9264	0.9270	0.9018	0.8745	0.9655	0.9858	0.9963
CC	0.9061	0.8828	0.8341	0.8232	0.9348	0.9786	0.9810
LPC	0.9241	0.9248	0.8984	0.8746	0.9670	0.9867	0.9923

Table 3. Comparative analysis of F1 score values for various network topological features across multiple frequency bands.

Feature	Frequency Band						
	Delta	**Theta**	**Alpha1**	**Alpha2**	**Beta1**	**Beta2**	**Gamma**
Degree	0.8786	0.8637	0.8532	0.8468	0.9274	0.9676	0.9774
PL	0.7473	0.7130	0.6993	0.6714	0.7280	0.7896	0.8199
EC	0.8443	0.8305	0.8022	0.7563	0.9055	0.9568	0.9704
CC	0.8201	0.7917	0.7362	0.7149	0.8412	0.9277	0.9378
LPC	0.8454	0.8304	0.8022	0.7536	0.9008	0.9581	0.9751

Among the global topological features, the clustering coefficient (CC) emerges as the most effective classifier across all frequency bands. The classification accuracy ranges from a peak of 0.9407 in the Gamma band to a minimum of 0.7419 in the Alpha2 band. Regarding local topological features, the node degree shows the highest classification performance throughout the frequency band, achieving a maximum accuracy of 0.9782 in the Gamma band and maintaining a minimum accuracy of 0.8500 even in the least performing Alpha2 band. This consistent performance pattern across both global and local features underscores the robustness of these topological measures in network classification tasks.

3.2. Comparative Analysis of Classification Performance with Alternative Spatial Cognitive Electroencephalogram (EEG) Feature Extraction Models

To evaluate the effectiveness of the proposed CFENG in classifying spatial cognitive electroencephalogram (EEG) signals, a comparative analysis involving five alternative methods across seven frequency bands was conducted, as shown in Tables 4–6. These five EEG analysis methods include three deep learning models and two classical feature extraction models. Specifically, the three deep learning models are the Multi-Scale Attention

Residual Network (MSARN), Separable 1D Convolution (SepConv1D), and EEGNet. The two classical feature extraction models are Common Spatial Patterns (CSPs) and Power Spectral Density (PSD), both evaluated using Random Forest. Below is a brief description of these five EEG analysis methods.

Table 4. Comparative analysis of classification accuracy for various spatial cognitive EEG feature extraction models across multiple frequency bands.

Model	Frequency Band						
	Delta	Theta	Alpha1	Alpha2	Beta1	Beta2	Gamma
CFENG	0.89	0.87	0.86	0.85	0.92	0.96	0.98
PSD+RF	0.86	0.80	0.83	0.76	0.86	0.86	0.91
CSP+RF	0.77	0.81	0.77	0.79	0.82	0.86	0.88
MSARN	0.82	0.81	0.75	0.75	0.87	0.93	0.97
SepConv1D	0.78	0.80	0.73	0.76	0.82	0.84	0.90
EEGNet	0.85	0.86	0.85	0.85	0.91	0.97	0.96

Table 5. Comparative analysis of AUC values for various spatial cognitive EEG feature extraction models across multiple frequency bands.

Model	Frequency Band						
	Delta	Theta	Alpha1	Alpha2	Beta1	Beta2	Gamma
CFENG	0.95	0.94	0.93	0.92	0.98	0.99	1.00
PSD+RF	0.85	0.80	0.83	0.76	0.86	0.85	0.91
CSP+RF	0.86	0.90	0.86	0.87	0.91	0.95	0.95
MSARN	0.81	0.79	0.75	0.73	0.86	0.93	0.97
SepConv1D	0.75	0.78	0.66	0.73	0.80	0.82	0.87
EEGNet	0.96	0.96	0.94	0.93	0.98	0.99	0.99

Table 6. Comparative analysis of F1 score values for various spatial cognitive EEG feature extraction models across multiple frequency bands.

Model	Frequency Band						
	Delta	Theta	Alpha1	Alpha2	Beta1	Beta2	Gamma
CFENG	0.88	0.87	0.85	0.85	0.92	0.96	0.98
PSD+RF	0.86	0.79	0.82	0.76	0.85	0.84	0.90
CSP+RF	0.77	0.81	0.77	0.79	0.82	0.86	0.88
MSARN	0.81	0.76	0.77	0.72	0.86	0.93	0.97
SepConv1D	0.71	0.77	0.57	0.69	0.78	0.76	0.80
EEGNet	0.85	0.85	0.85	0.85	0.91	0.97	0.96

CSP [32] is a classical technique for EEG signal analysis, extracting discriminative spatial features by maximizing variance differences between two signal classes. It is ideal for dimensionality reduction and binary classification tasks like spatial cognitive EEG analysis [8]. PSD analyzes EEG frequency components by calculating energy distribution across frequencies, characterizing spectral properties. It is widely used for extracting frequency-domain features in BCI tasks [33]. SepConv1D [34] is a lightweight method that decomposes standard convolution into depthwise and pointwise operations, reducing computational load while maintaining feature extraction. It efficiently extracts temporal features from EEG signals. MSARN [35] integrates multi-scale feature extraction, attention mechanisms, and residual learning to extract spatiotemporal EEG features, focusing on task-relevant brain regions or frequency bands. EEGNet [36] is a lightweight model combining depthwise separable and temporal convolutions to efficiently extract spatiotemporal EEG features, making it suitable for various BCI tasks.

As shown in Tables 4–6, the proposed CFENG model demonstrates superior classification performance across all seven frequency bands, with classification accuracies of 0.89, 0.87, 0.86, 0.85, 0.92, 0.96, and 0.98, respectively. In comparison, MSARN, the best-performing deep learning model, achieves classification accuracies of 0.82, 0.81, 0.75, 0.75, 0.87, 0.93, and 0.97 in the same frequency bands. Notably, CFENG outperforms MSARN across all frequency bands, particularly in the Delta, Theta, Alpha1, and Alpha2 bands. Furthermore, CFENG surpasses the two classical feature extraction models (CSP and PSD) in all frequency bands.

3.3. Comparative Analysis of Classifier Performance

In the subsequent parameter ablation test, we employed the XGBoost classifier to mitigate the impact of the classifier on parameter selection. Tables 7–9 illustrate the classification performance of XGBoost in comparison to eight other classifiers.

Table 7. Comparative analysis of classification accuracy for various classifiers across multiple frequency bands.

Model	Frequency Band						
	Delta	**Theta**	**Alpha1**	**Alpha2**	**Beta1**	**Beta2**	**Gamma**
xgboost	0.8810	0.8657	0.8557	0.8500	0.9294	0.9687	0.9782
knn	0.8819	0.8551	0.8375	0.8423	0.9102	0.9695	0.9751
rf	0.8770	0.8541	0.8332	0.8370	0.9049	0.9562	0.9685
gbc	0.8738	0.8482	0.8327	0.8311	0.8969	0.9503	0.9626
mlp	0.8615	0.8439	0.8124	0.8103	0.8797	0.9327	0.9530
dt	0.8498	0.8209	0.8049	0.7819	0.8664	0.9289	0.9471
ada	0.8225	0.7878	0.7734	0.7568	0.8610	0.9060	0.9455
lda	0.7937	0.7386	0.7504	0.7488	0.7659	0.8455	0.8947
svm	0.7419	0.6114	0.6120	0.5430	0.7082	0.7194	0.6606

Table 8. Comparative analysis of AUC values for various classifiers across multiple frequency bands.

Model	Frequency Band						
	Delta	**Theta**	**Alpha1**	**Alpha2**	**Beta1**	**Beta2**	**Gamma**
xgboost	0.9523	0.9422	0.9303	0.9288	0.9800	0.9928	0.9965
knn	0.9508	0.9277	0.9200	0.9170	0.9626	0.9903	0.9962
rf	0.9425	0.9278	0.9090	0.9085	0.9686	0.9906	0.9959
gbc	0.9457	0.9284	0.9136	0.9041	0.9609	0.9832	0.9917
mlp	0.9266	0.9176	0.8907	0.8804	0.9483	0.9763	0.9807
dt	0.9287	0.8968	0.8911	0.8897	0.8663	0.9289	0.9472
ada	0.8221	0.7875	0.7732	0.7566	0.9427	0.9732	0.9856
lda	0.9176	0.8134	0.8221	0.8261	0.8550	0.9406	0.9633
svm	0.8042	0.8554	0.8492	0.8218	0.0000	0.0000	0.0000

The choice of classifier does not influence the sorting performance across various frequency bands. Regardless of the classifier selected, its classification performance across the seven frequency bands, ranked from highest to lowest, is as follows: Gamma band, Beta2 band, Beta1 band, Delta band, Theta band, Alpha1 band, and Alpha2 band.

By comparing the selection of various frequency bands and classifiers, the XGBoost classifier demonstrates the highest classification accuracy within the Gamma band.

Overall, the XGBoost classifier demonstrates superior performance compared to other models. With the exception of the Beta2 band, it achieves the highest accuracy, AUC, and F1 score across the remaining six bands. Notably, in the Beta2 band, the AUC remains the highest among all classifiers. Consequently, it is justifiable to select XGBoost as the preferred classifier for this analysis.

Table 9. Comparative analysis of F1 score values for various classifiers across multiple frequency bands.

	Frequency Band						
	Delta	**Theta**	**Alpha1**	**Alpha2**	**Beta1**	**Beta2**	**Gamma**
xgboost	0.8786	0.8637	0.8532	0.8468	0.9274	0.9676	0.9774
knn	0.8807	0.8539	0.8365	0.8400	0.9072	0.9685	0.9742
rf	0.8754	0.8549	0.8287	0.8311	0.9025	0.9544	0.9674
gbc	0.8726	0.8364	0.8311	0.8286	0.8938	0.9482	0.9613
mlp	0.8583	0.8435	0.8044	0.8052	0.8829	0.9295	0.9514
dt	0.8501	0.8194	0.8028	0.7577	0.8624	0.9268	0.9457
ada	0.8149	0.7801	0.7656	0.7483	0.8587	0.9001	0.9430
lda	0.7517	0.7592	0.7686	0.7697	0.7823	0.8568	0.8987
svm	0.7630	0.3505	0.3371	0.1098	0.6360	0.6431	0.5656

3.4. Comparative Analysis of the Performance of Various Cross Entropy Methods

Tables 10–12 present a comparative analysis of the classification outcomes derived from five distinct cross entropy measures utilized as connection matrices among various EEG channels. The findings are detailed as follows:

1. The classification performance of cross entropy across the seven frequency bands, ranked from highest to lowest, is as follows: Gamma band, Beta2 band, Beta1 band, Delta band, Theta band, Alpha1 band, and Alpha2 band.
2. In all seven frequency bands, cross fuzzy entropy demonstrates superior classification performance, followed closely by cross conditional entropy.
3. Cross fuzzy entropy demonstrates the highest classification accuracy within the Gamma band, while exhibiting the lowest classification accuracy in the Alpha2 band. These findings are consistent across other performance indicators as well.

Table 10. Comparative analysis of classification accuracy for various cross entropy methods across multiple frequency bands.

Entropy	Frequency Band						
	Delta	**Theta**	**Alpha1**	**Alpha2**	**Beta1**	**Beta2**	**Gamma**
Cross fuzzy entropy	0.8810	0.8657	0.8557	0.8500	0.9294	0.9687	0.9782
Cross sample entropy	0.6291	0.6136	0.5708	0.5500	0.6141	0.5885	0.7461
Cross permutation entropy	0.5762	0.5954	0.6056	0.6809	0.7220	0.8204	0.8856
Cross spectrum entropy	0.5842	0.5499	0.5318	0.5489	0.5430	0.5799	0.6461
Cross conditional entropy	0.7242	0.7434	0.6969	0.7156	0.8338	0.8814	0.9337

Table 11. Comparative analysis of AUC values for various cross entropy methods across multiple frequency bands.

Entropy	Frequency Band						
	Delta	**Theta**	**Alpha1**	**Alpha2**	**Beta1**	**Beta2**	**Gamma**
Cross fuzzy entropy	0.9517	0.9391	0.9274	0.9218	0.9773	0.9914	0.9963
Cross sample entropy	0.6732	0.6668	0.5991	0.5675	0.6368	0.6237	0.8193
Cross permutation entropy	0.6035	0.6360	0.6353	0.7474	0.7935	0.8929	0.9506
Cross spectrum entropy	0.6175	0.5816	0.5483	0.5541	0.5724	0.6201	0.7225
Cross conditional entropy	0.7911	0.8053	0.7595	0.7789	0.9024	0.9425	0.9769

Table 12. Comparative analysis of F1 score values for various cross entropy methods across multiple frequency bands.

Entropy	Frequency Band						
	Delta	**Theta**	**Alpha1**	**Alpha2**	**Beta1**	**Beta2**	**Gamma**
Cross fuzzy entropy	0.8786	0.8637	0.8532	0.8468	0.9274	0.9676	0.9774
Cross sample entropy	0.5618	0.5717	0.5288	0.5208	0.5545	0.5444	0.7278
Cross permutation entropy	0.5476	0.6020	0.6215	0.6802	0.7221	0.8156	0.8846
Cross spectrum entropy	0.4698	0.4750	0.4335	0.4351	0.4140	0.4766	0.5967
Cross conditional entropy	0.7251	0.7419	0.7013	0.7090	0.8298	0.8773	0.9314

3.5. Selection of Network Parameters for Electroencephalogram (EEG) Functional Connectivity

In the preceding section, we selected the cross fuzzy entropy that exhibited optimal classification performance to serve as the connection matrix for the EEG functional connectivity network. In this section, we will further examine the influence of various parameters on classification performance, with a primary focus on the embedding dimension and time delay.

3.5.1. Selection of Embedding Dimensions

Tables 13–15 present a comparative analysis of the brain functional connectivity networks derived from four distinct embedding dimensions across multiple frequency bands. The findings are detailed as follows:

Table 13. Comparative analysis of brain functional connectivity networks with classification accuracy for different embedding dimensions across multiple frequency bands.

Embedding Dimension	Frequency Band						
	Delta	**Theta**	**Alpha1**	**Alpha2**	**Beta1**	**Beta2**	**Gamma**
1	0.8755	0.8755	0.8503	0.8455	0.9240	0.9674	0.9726
2	0.8810	0.8657	0.8557	0.8500	0.9294	0.9687	0.9782
3	0.8845	0.8658	0.8525	0.8535	0.9156	0.9615	0.9701
4	0.8717	0.8680	0.8493	0.8546	0.9043	0.9653	0.9711

Table 14. Comparative analysis of AUC values for brain functional connectivity networks with different embedding dimensions across multiple frequency bands.

Embedding Dimension	Frequency Band						
	Delta	**Theta**	**Alpha1**	**Alpha2**	**Beta1**	**Beta2**	**Gamma**
1	0.9520	0.9419	0.9253	0.9221	0.9739	0.9916	0.9949
2	0.9523	0.9422	0.9303	0.9288	0.9800	0.9928	0.9965
3	0.9514	0.9406	0.9275	0.9216	0.9772	0.9913	0.9949
4	0.9522	0.9418	0.9264	0.9296	0.9682	0.9928	0.9947

Table 15. Comparative analysis of F1 score values for brain functional connectivity networks with different embedding dimensions across multiple frequency bands.

Embedding Dimension	Frequency Band						
	Delta	**Theta**	**Alpha1**	**Alpha2**	**Beta1**	**Beta2**	**Gamma**
1	0.8724	0.8740	0.8478	0.8443	0.9213	0.9663	0.9715
2	0.8786	0.8637	0.8532	0.8468	0.9274	0.9676	0.9774
3	0.8819	0.8651	0.8504	0.8512	0.9130	0.9599	0.9690
4	0.8681	0.8677	0.8469	0.8513	0.9024	0.9641	0.9701

(1) The choice of embedding dimensions does not influence the ranking of classification performance across various frequency bands. Regardless of the embedding dimension employed, the classification performance across the seven frequency bands, ordered from highest to lowest, is as follows: Gamma band, Beta2 band, Beta1 band, Delta band, Theta band, Alpha1 band, and Alpha2 band.

(2) In the five frequency bands—Delta, Alpha1, Beta1, Beta2, and Gamma—the classification performance is optimized at an embedding dimension of 2. Conversely, in the Theta frequency bands, the classification performance is maximized at an embedding dimension of 1.

(3) By analyzing the selection of various frequency bands and embedding dimensions, it has been determined that the highest classification accuracy is achieved in the Gamma band when the embedding dimension is set to 2.

3.5.2. Selection of Delays

Tables 16–18 present a comparative analysis of the brain functional connectivity networks derived from four distinct delays across multiple frequency bands. The findings are detailed as follows:

Table 16. Comparative analysis of classification accuracy for brain functional connectivity networks with different embedding dimensions across multiple frequency bands.

Delay	Frequency Band						
	Delta	**Theta**	**Alpha1**	**Alpha2**	**Beta1**	**Beta2**	**Gamma**
1	0.8810	0.8657	0.8557	0.8500	0.9294	0.9687	0.9782
2	0.8883	0.8626	0.8567	0.8514	0.9188	0.9669	0.9727
3	0.8835	0.8593	0.8504	0.8434	0.8963	0.9679	0.9679
4	0.8904	0.8765	0.8466	0.8332	0.9161	0.9514	0.9743

Table 17. Comparative analysis of AUC values for brain functional connectivity networks with different embedding dimensions across multiple frequency bands.

Delay	Frequency Band						
	Delta	**Theta**	**Alpha1**	**Alpha2**	**Beta1**	**Beta2**	**Gamma**
1	0.9523	0.9422	0.9303	0.9288	0.9800	0.9928	0.9965
2	0.9538	0.9371	0.9282	0.9278	0.9750	0.9911	0.9960
3	0.9537	0.9244	0.9248	0.9214	0.9678	0.9923	0.9921
4	0.9530	0.9458	0.9272	0.9174	0.9752	0.9878	0.9956

Table 18. Comparative analysis of F1 score values for brain functional connectivity networks with different embedding dimensions across multiple frequency bands.

Delay	Frequency Band						
	Delta	**Theta**	**Alpha1**	**Alpha2**	**Beta1**	**Beta2**	**Gamma**
1	0.8786	0.8637	0.8532	0.8468	0.9274	0.9676	0.9774
2	0.8858	0.8616	0.8551	0.8467	0.9163	0.9655	0.9718
3	0.8806	0.8549	0.8481	0.8415	0.8938	0.9667	0.9667
4	0.8877	0.8744	0.8442	0.8296	0.9131	0.9494	0.9734

(1) The selection of delay does not influence the sorting performance across various frequency bands. Independent of the delay, the classification performance in the seven frequency bands, ranked from highest to lowest, is as follows: Gamma band, Beta2 band, Beta1 band, Delta band, Theta band, Alpha1 band, and Alpha2 band.

(2) In the three frequency bands (Beta1 band, Beta2 band, and Gamma band), the classification performance is optimal when the delay is set to 1.

(3) By comparing the selection of various frequency bands and delays, the highest classification accuracy is achieved in the Gamma band when the delay is set to 1.

3.6. Comparative Analysis of the Classification Performance of Various Electroencephalogram (EEG) Functional Connectivity Measures

To demonstrate the superiority of cross fuzzy entropy (XFuzzEn) over other classical EEG network measures in classification tasks, a comparative analysis was conducted on several widely-used EEG functional connectivity measures. These included magnitude-squared coherence (MSC), phase-locking value (PLV), phase lag index (PLI), imaginary part of coherence (ImCoh), and Granger causality (GC). These methods each have their specific focus and are suitable for different scenarios in EEG signal analysis.

Magnitude Squared Coherence [37]: MSC measures the linear correlation between two signals in the frequency domain, with values ranging from 0 to 1. It is used to assess the synchrony between different brain regions at specific frequencies.

Phase Locking Value [38]: PLV evaluates the phase synchronization between two signals, with values ranging from 0 to 1. It is commonly used to study phase-locking phenomena between brain regions.

Phase Lag Index [39]: PLI calculates the asymmetry of phase differences to reduce the impact of instantaneous synchrony, with values ranging from 0 to 1. It is applied to detect phase lag relationships between brain regions while avoiding spurious synchrony.

Imaginary Part of the Coherence [40]: ImCoh represents the imaginary component of coherence, which helps reduce the influence of zero-lag synchrony. It is used to investigate time-lagged synchrony between brain regions.

Granger Causality [1,26]: GC assesses whether one signal has a causal influence on another by analyzing time series predictions. It is widely used to examine information flow and causality between brain regions.

Statistical analysis of the results, presented in Table 19, reveals that the proposed Cross Fuzzy Entropy Network Graph (CFENG)-based model delivered the highest performance in classifying spatial cognitive EEG signals, whereas PLI exhibited the poorest performance. Figure 5 provides a detailed distribution of classification accuracy across various brain functional connectivity networks, clearly showing that the CFENG model achieved a significantly higher accuracy compared to other models, with a statistically notable difference.

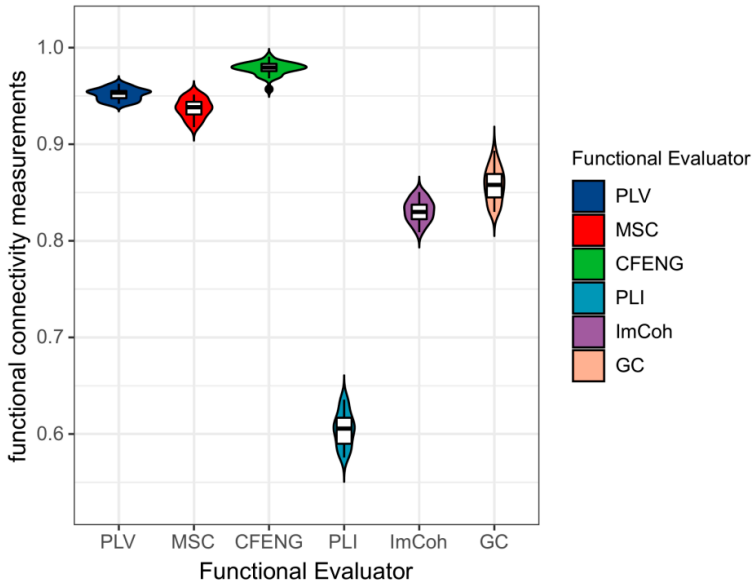

Figure 5. Comparison of classification accuracy for different brain functional connectivity networks.

Table 19. Comparison of classification performance for different brain functional connectivity networks.

Features	Accuracy	F1 Score	AUC
CFENG	0.9782 ± 0.0069	0.9774 ± 0.0071	0.9965 ± 0.0019
PLV	0.9516 ± 0.0062	0.9487 ± 0.0067	0.9886 ± 0.0041
PLI	0.6048 ± 0.0178	0.5841 ± 0.0256	0.6471 ± 0.0195
MSC	0.9371 ± 0.0100	0.9342 ± 0.0102	0.9813 ± 0.0041
ImCoh	0.8310 ± 0.0116	0.8252 ± 0.0131	0.9097 ± 0.0117
GC	0.8577 ± 0.0175	0.8527 ± 0.0184	0.9356 ± 0.0099

3.7. Reproducibility Analysis of Results Using Different Electroencephalogram (EEG) Preprocessing Techniques

The reproducibility of results may be influenced by the use of different EEG preprocessing techniques. In this study, we employed a standard EEG preprocessing pipeline, which included filtering, artifact removal, re-referencing, baseline correction, and epoch segmentation. Except for the epoch segmentation step, all other procedures were based on well-established methods in the EEG analysis, such as 1–50 Hz bandpass filtering, independent component analysis, and common average reference. Previous research has shown that these methods have minimal impact on the results. However, the choice of sliding window size during epoch segmentation can significantly affect the number of samples and, consequently, the reproducibility of the results.

In this study, epoch segmentation was performed using a 2-s sliding window, following prior research. To investigate the impact of different sliding window sizes on the results, we also tested a 4-s sliding window. Apart from the window size, all other steps in the EEG preprocessing pipeline remained identical. As shown in Figures 6 and 7, the ranking of classification accuracy across frequency bands was consistent between the 2-s (Figure 6) and 4-s (Figure 7) sliding windows. Specifically, the Gamma band achieved the highest classification accuracy, followed by Beta2, Beta1, Delta, Theta, Alpha1, and Alpha2 bands. Furthermore, as illustrated in Figure 8, a *t*-test comparing the classification accuracy of the Gamma band between the two sliding window sizes revealed no statistically significant difference.

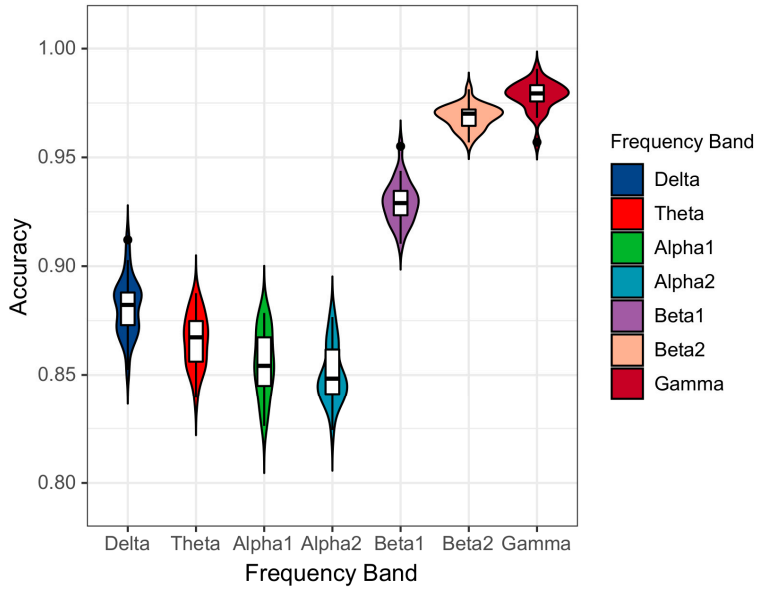

Figure 6. Classification accuracy across seven different frequency bands using a 2-s sliding window size.

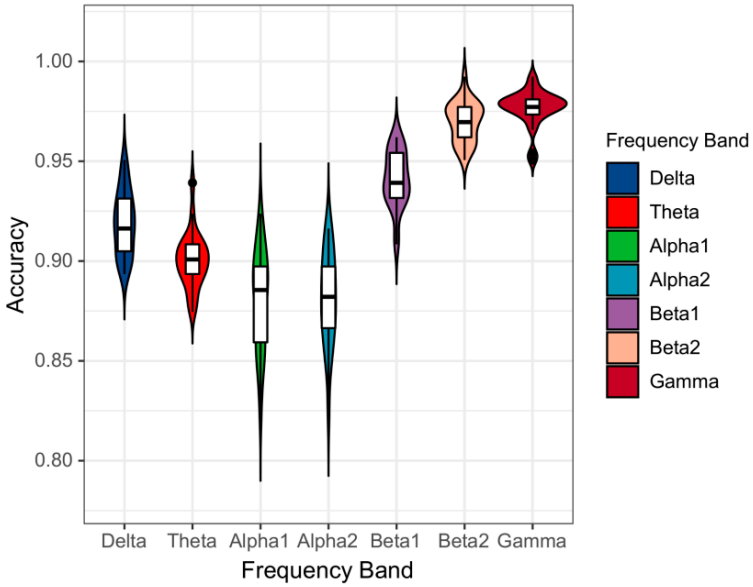

Figure 7. Classification accuracy across seven different frequency bands using a 4-s sliding window size.

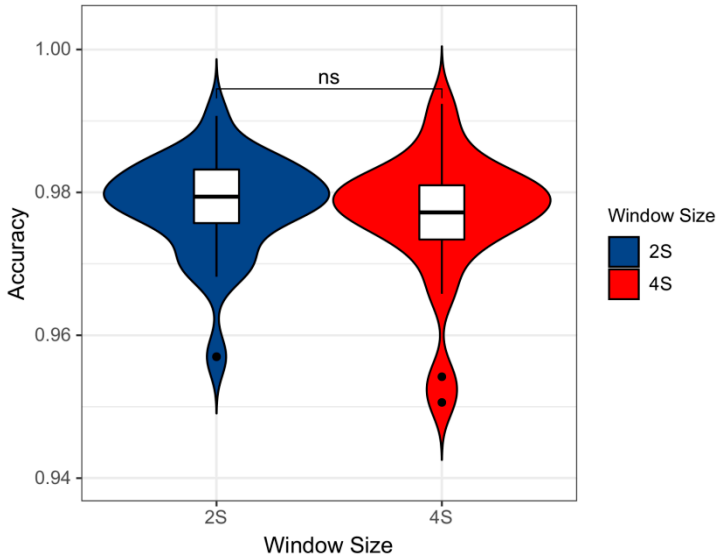

Figure 8. Comparison of classification accuracy in the Gamma band for sliding window sizes of 2 s and 4 s. The results indicate no statistically significant difference between the two groups.

Based on these findings, we conclude that adjusting the sliding window size within a reasonable range during epoch segmentation, as part of the standard EEG preprocessing pipeline, can yield reproducible results. However, further research is needed to define the appropriate range for sliding window sizes in epoch segmentation to ensure robust and generalizable outcomes.

3.8. Comparative Analysis of the Significance of Electroencephalogram (EEG) Channels Across Various Frequency Bands

We employed Shapley Additive Explanations (SHAPs) [41] to assess the significance of EEG channels across various frequency bands. Figures 9–15 illustrate the importance ranking of each channel within each frequency band, along with the distribution of their SHAP values. In the Delta band, the channels exhibiting an importance greater than 0.05, listed in descending order, are Fp1, O1, P7, P8, and Cz. In the Theta band, the channels with an importance exceeding 0.05, also in descending order, are Fp1, P8, and O1. For

the Alpha1 band, the channels surpassing the 0.05 importance threshold, in descending order, are P8, Fp1, and O1. In the Alpha2 band, the channels with an importance greater than 0.05, listed in descending order, are P8, Fp1, Cz, O1, and C4. In the Beta1 band, the channels whose importance exceeds 0.05, in descending order, are Cz, P8, O1, Fp1, and C4. In the Beta2 band, the channels with an importance greater than 0.05, also in descending order, are Cz, O1, C4, and Fp1. In the Gamma band, the channels exhibiting an importance greater than 0.05, in descending order, are Cz, C4, and O1. Across the seven frequency bands analyzed, Fp1 is identified as the most significant channel in both the Delta and Theta bands, P8 is the most significant channel in the Alpha1 and Alpha2 bands, and Cz is the most significant channel in the Beta1, Beta2, and Gamma bands. From the analysis above, it can be seen that the contributions of EEG channels with left–right symmetric distribution to the classification of spatial cognitive signals are different.

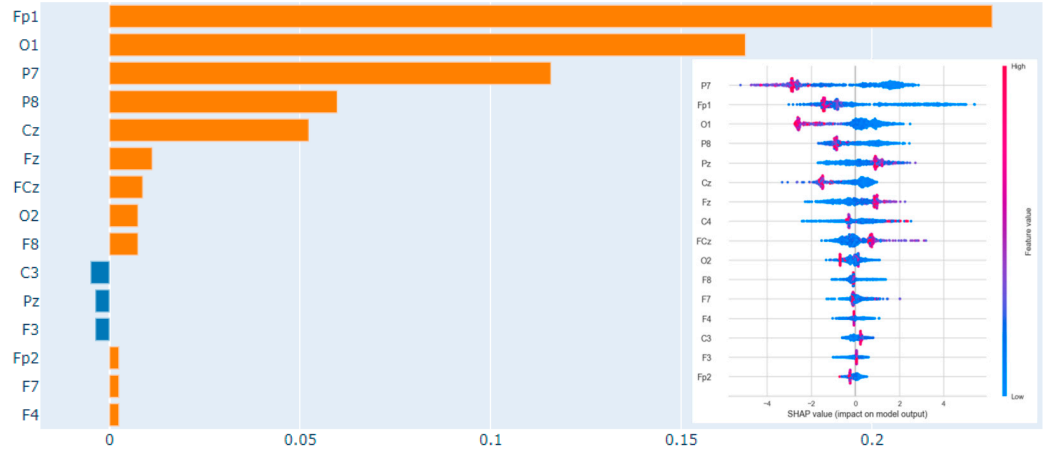

Figure 9. Permutation feature importance and summary plot of EEG channels using SHAP in the Delta frequency band.

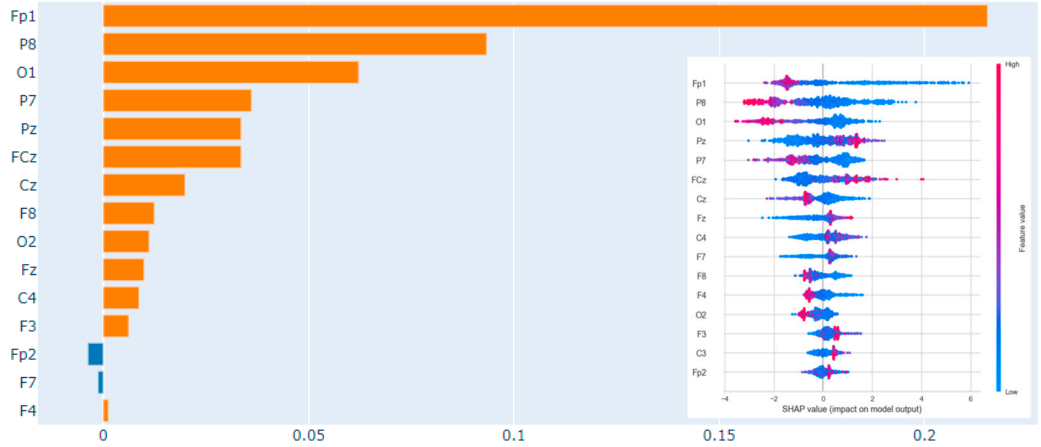

Figure 10. Permutation feature importance and summary plot of EEG channels using SHAP in the Theta frequency band.

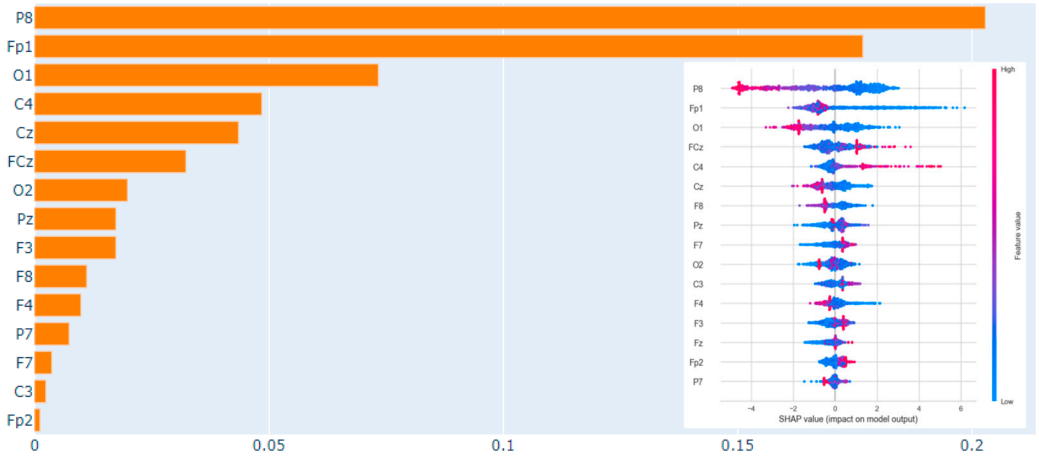

Figure 11. Permutation feature importance and summary plot of EEG channels using SHAP in the Alpha1 frequency band.

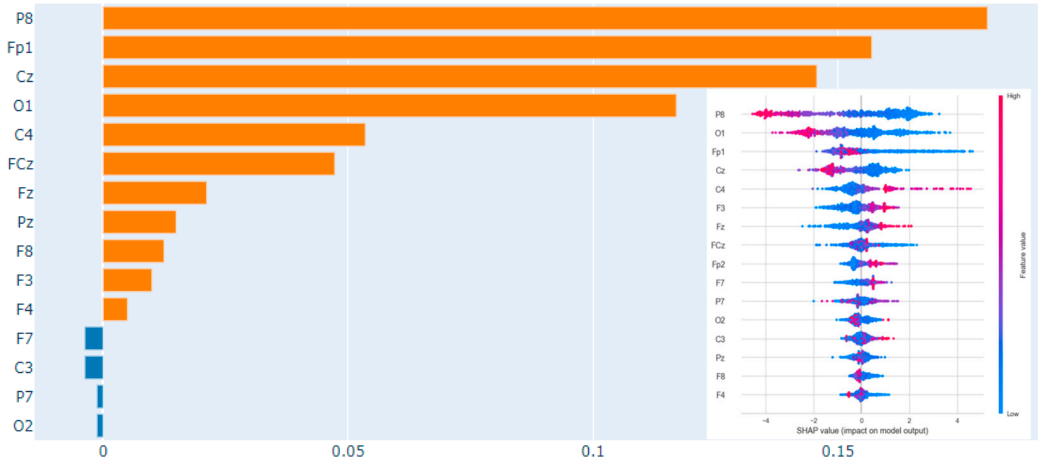

Figure 12. Permutation feature importance and summary plot of EEG channels using SHAP in the Alpha2 frequency band.

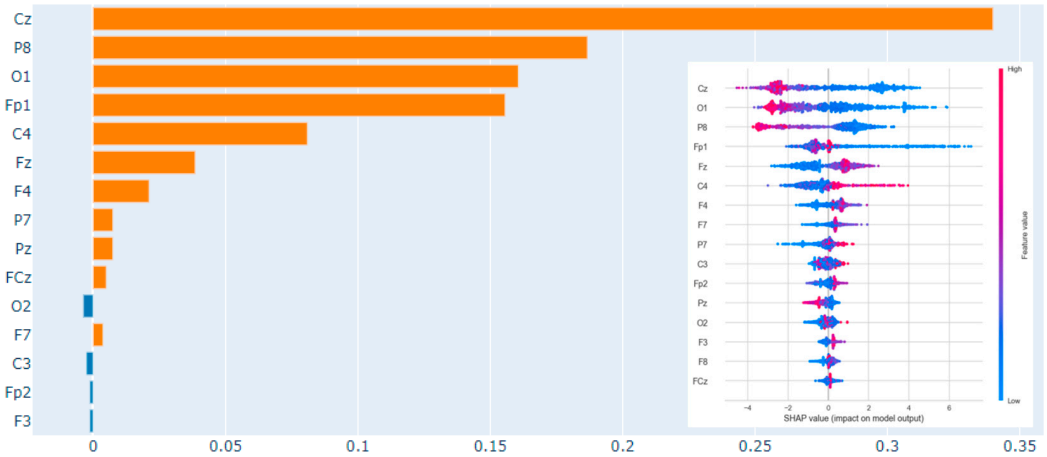

Figure 13. Permutation feature importance and summary plot of EEG channels using SHAP in the Beta1 frequency band.

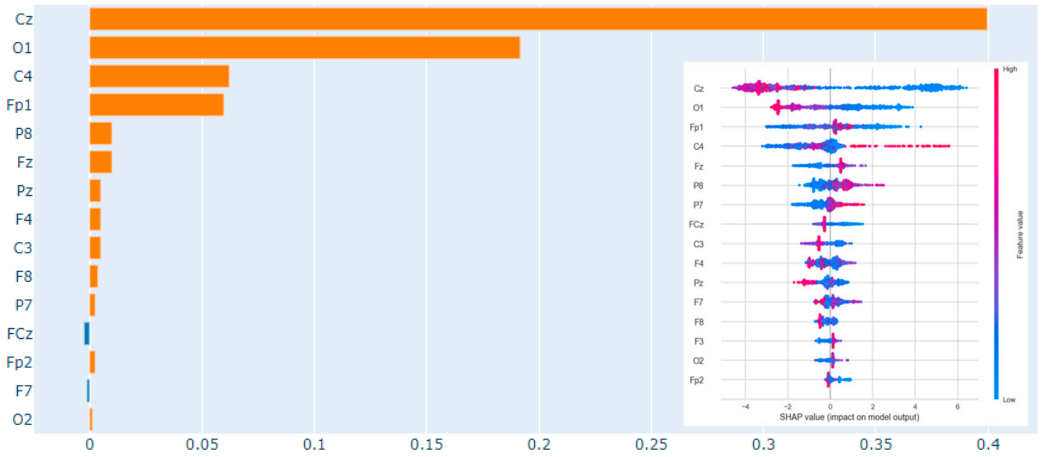

Figure 14. Permutation feature importance and summary plot of EEG channels using SHAP in the Beta2 frequency band.

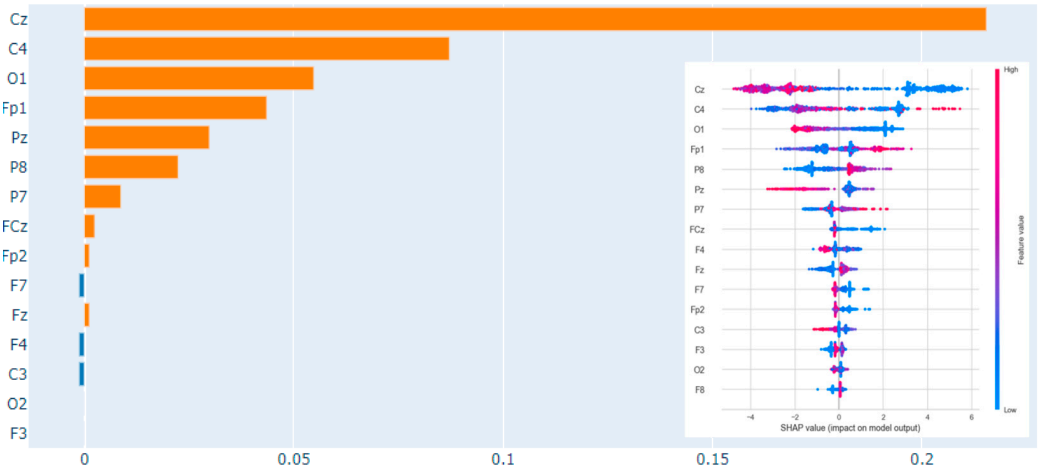

Figure 15. Permutation feature importance and summary plot of EEG channels using SHAP in the Gamma frequency band.

The Gamma band and the Cz channel, which exhibited the highest classification performance, were selected for analysis. A comparative examination of the data distribution pertaining to five network topological features across two spatial cognitive EEG assessments is presented in Figure 16. Following a 28-day period of spatial cognitive training, notable changes were observed in the data distribution of the five network topological features within the EEG signals collected before and after the training sessions, with both comparisons yielding statistically significant results. Specifically, the mean values of the clustering coefficient, eigenvector centrality, and Laplacian centrality demonstrated an increase, whereas the mean values of degree and eigenpath length exhibited a decrease. Furthermore, the standard deviation of all five network topological features was reduced, indicating a more clustered data distribution.

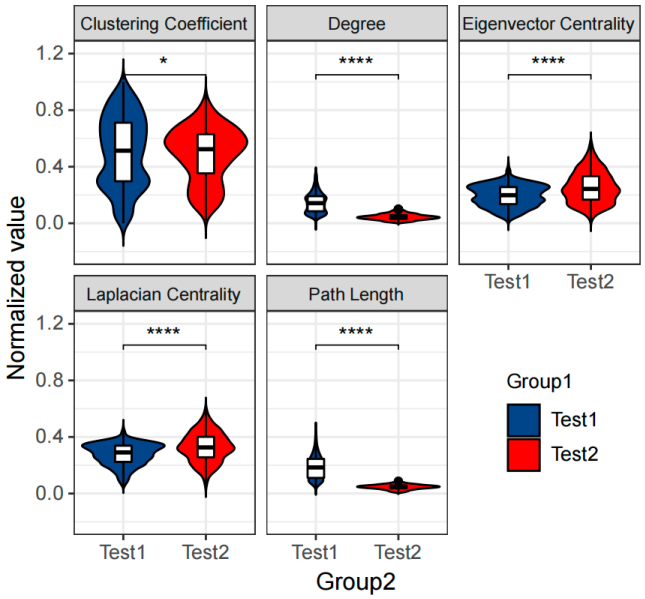

Figure 16. Comparison of data distribution in two spatial cognitive EEG tests for five network topology features. The symbols * and **** indicate statistical significance levels (*p*-values), with * representing $p < 0.05$ and **** representing $p < 0.0001$.

4. Discussion

This study employs classification to assess the effectiveness of VR-based spatial cognitive training by analyzing EEG signals recorded before and after the intervention. Specifically, it aims to distinguish between pre-training and post-training states using network topology features (e.g., degree, clustering coefficient, characteristic path length) extracted from EEG data. This approach identifies the most discriminative features, shedding light on the neural mechanisms underlying training effects. Additionally, the classification task quantifies training-induced changes in brain functional connectivity, revealing key neural markers of cognitive improvement. This method provides a robust and interpretable framework for evaluating spatial cognitive performance, with significant implications for both spatial cognitive training and clinical diagnostics.

In this study, we propose a classification model for spatially cognitive EEG signals based on the topological features of functionally connected networks. The EEG functional connectivity networks were constructed using statistical dependencies between different EEG channels, and we compared the network topological features across various frequency bands. To evaluate the importance of different EEG channels, we employed the SHAP framework with XGBoost as the classifier. We conducted a comprehensive analysis on a spatial cognitive EEG dataset collected during VR games, comparing the performance of our proposed model with other methods. Additionally, we examined the impact of different adjacency matrices on the construction of the EEG functional connection network, evaluated various parameters of the adjacency matrix, compared different network topological features, and assessed the performance of different classifiers and the significance of EEG channels. The rationality and validity of our research findings, as well as the prospects for future research, are discussed in detail in the subsequent section.

4.1. Comparative Analysis of the Various Network Topology Features

In our study, we categorized network topology features into two types: global and local features, as outlined in previous literature [26]. Local features primarily reflect the centrality of individual nodes (EEG channels) within the network, indicating the significance of the corresponding local brain region's function. Global features, on the other

hand, are used to measure the functional integration of various brain regions and provide insights into the global communication efficiency among all nodes. Our results, presented in Tables 1–3, indicate that the clustering coefficient exhibits superior classification performance compared to the feature path length among global features. This observation is attributed to the fact that spatial cognitive functions are often localized to specific brain regions, and classification relies more on functional centrality than on the efficiency of information flow. Specifically, the feature path length primarily reflects the overall propagation efficiency of information within the network, whereas the clustering coefficient highlights the aggregation or centrality of information. Among local features, the degree consistently outperformed eigenvector centrality and Laplacian centrality, particularly in the Delta, Theta, Alpha1, and Alpha2 frequency bands. However, in the Beta1, Beta2, and Gamma bands, the classification performance of these three features was comparable, with the highest classification accuracy in the Gamma band being 0.9782, 0.9711, and 0.9759, respectively. This result is attributed to the fact that degree, eigenvector centrality, and Laplacian centrality all represent node centrality, with the primary difference being the aspects of centrality. The broader applicability of the degree is also consistent with the findings of other EEG classification studies based on graph theory indices [26,42]. Furthermore, as shown in Figure 16, after 28 days of spatial cognitive training, we observed an increase in the mean values of clustering coefficient, eigenvector centrality, and Laplacian centrality, while the mean values of feature path lengths decreased. The distribution of all five network topological features became more clustered, suggesting that the VR game training used in this study enhanced the functional centrality of brain regions related to spatial cognition and reduced the path length of information flow. These findings validate the feasibility of spatial cognitive training through specific VR games from the perspective of brain functional connectivity.

4.2. Comparative Analysis of Various Spatial Cognitive Electroencephalogram (EEG) Feature Extraction Methods

The performance of the EEG functional connectivity network topological features proposed in this study, when applied to spatial cognitive EEG signal classification, surpasses existing models across all seven frequency bands. This superiority is evident when compared to machine learning models based on PSD and various time-domain deep learning methods, as demonstrated in Tables 4–6. Spatial cognitive EEG signals are elicited by complex tasks and are intricately linked to the functionality of multiple brain regions. The use of a single PSD in the frequency domain and various time-domain features alone is insufficient to comprehensively characterize the functional connections among multiple brain regions in such complex paradigms. In contrast to spatial cognitive EEG signal classification methods based on multi-dimensional conditional mutual information and arrangement conditional mutual information [8,9], our proposed method demonstrates comparable performance, achieving a peak classification accuracy of 98%. This comparable performance can be attributed to the fact that both methods rely on the sequence similarity between brain electrical channels, which enables them to effectively represent the functional connectivity of brain regions. Furthermore, our method advances by providing additional insights through the analysis of the importance of different frequency bands and channels using network topological features. This analysis enhances the interpretability of our model, contributing to a deeper understanding of the underlying neural mechanisms involved in spatial cognitive processes.

4.3. Comparative Analysis of the Performance of Various Adjacency Matrices Constituting the Functional Electroencephalogram (EEG) Connectivity Network

In the construction of EEG functional connectivity networks, a common approach in numerous studies [26] involves the use of threshold values to binarize weights, thereby neglecting weak connections and resulting in powerless networks. However, considering the complexity of spatial cognitive processes in VR games and the multi-centrality of brain functional connections, the exclusion of weak connections may adversely affect the accurate measurement of node centrality. Therefore, this study employs cross fuzzy entropy as the adjacency matrix, utilizing its values as the weights of edges between nodes, and constructs the EEG functional connectivity network as a weighted directed graph.

As shown in Tables 10–12, the classification performance of cross fuzzy entropy surpasses that of other cross entropies. Specifically, the highest classification accuracy achieved using cross fuzzy entropy is 0.98, followed by cross condition entropy at 0.93, and cross spectrum entropy at 0.65. The advantage of cross fuzzy entropy lies in its robustness to noise. It employs an exponential function to soften the similarity measure between two sequences and removes the influence of baseline drift through mean operation, resulting in entropy changes that are continuous and smooth with parameter variations. In contrast, other cross entropies measure similarity between sequences using the absolute difference and unit step function of the data, leading to sensitivity to threshold values and a lack of continuity in entropy values. Minor fluctuations or baseline drifts in data can cause abrupt changes in entropy values when using these methods. Consistent with these findings, related studies [23,43–45] have reported similar results, demonstrating a higher classification accuracy using fuzzy entropy for EEG signals from epileptic and non-epileptic patients compared to other entropies.

In addition to utilizing cross entropy as the adjacency matrix for EEG functional connectivity networks, previous studies [8,9] have adopted multi-dimensional conditional mutual information and its improved forms. The highest classification accuracy reported in these studies was 0.98 using a three-band composite method. An analysis of the three-band composite method used in these studies reveals that, despite varying combinations of frequency bands, the combination yielding the highest classification accuracy consistently includes the Gamma band. This finding aligns with the results obtained using cross fuzzy entropy in this study. However, the method proposed in this paper requires only a single band and does not necessitate band composition, resulting in simpler calculations and a more interpretable model.

As shown in Table 19 and Figure 5, the results demonstrate that cross fuzzy entropy provides superior classification performance compared to traditional brain functional network measures, such as MSC, PLI, PLV, ImCoh, and GC, due to its ability to capture non-linear dependencies and its robustness to noise, thereby justifying its use in this study. These advantages make cross fuzzy entropy particularly suitable for analyzing complex EEG signals, especially in the context of spatial cognitive training. Specifically, cross fuzzy entropy effectively captures non-linear relationships often overlooked by traditional linear measures, while its fuzzy similarity function reduces sensitivity to noise and data fluctuations, significantly enhancing reliability. This enables cross fuzzy entropy to characterize complex neural interactions and functional connectivity in brain networks more effectively. Unlike linear measures (e.g., MSC, GC) or phase-based methods (e.g., PLV, PLI, ImCoh), cross fuzzy entropy excels in capturing non-linear dynamics and maintaining robustness in noisy environments, establishing it as a superior tool for advanced brain network analysis. The findings are consistent with recent studies (e.g., Corsi et al., 2024 [46]), which emphasize the advantages of novel connectivity measures over traditional approaches. Future

studies should investigate the application of cross fuzzy entropy in other cognitive tasks and clinical settings to further validate its utility and generalize its effectiveness.

4.4. Parameter Selection of the Adjacency Matrix and Comparative Analysis of the Performance of Various Classifiers

The analysis presented in Tables 13–18 examines the impact of various parameters of cross fuzzy entropy, specifically embedding dimension and delay, on classification performance. The findings indicate that optimal performance is achieved when the embedding dimension is set to 2 and the delay is set to 1. The embedding dimension influences the length of the subsequence utilized for comparing local similarities between two sequences. As the embedding dimension decreases from a larger value to a smaller one, the focus of cross fuzzy entropy shifts from a global perspective to a more localized one. When the embedding dimension is reduced to one, the comparison between the two sequences occurs on a point-by-point basis. Given the complexity and lack of quasi-periodicity in spatial cognitive EEG signals, local features are found to be more representative than global features. The results suggest that the most effective local features are obtained with an embedding dimension of 2. The time delay parameter is defined as the downsampling of the original sequence in the context of cross fuzzy entropy, allowing for the comparison of similarities between the two sequences from a multi-scale perspective. However, since downsampling has already been applied during the preprocessing of EEG signals, variations in the delay parameters exert a limited influence on the outcomes. The results indicate that when the delay is set to 1, which corresponds to the absence of downsampling of the original sequence, the classification performance is optimal.

From Tables 7–9, it is evident that the selection of a classifier significantly influences the classification of spatial cognitive EEG signals when identical characteristics are employed. The XGBoost classifier demonstrates the highest performance, followed by the Random Forest Classifier, Gradient Boosting Classifier, KNN. In contrast, LDA and SVM with a linear kernel exhibit the poorest performance. This phenomenon can be attributed to the nonlinear nature of the topological features within the brain's functional connectivity network, which results in suboptimal classification outcomes for linear classifiers. Conversely, KNN, which relies on similarity measures, and boosting classification algorithms yield superior classification results. Notably, XGBoost further optimizes and enhances the performance of the boosting classifier, thereby achieving the best classification performance. Similar findings have been reported in other studies. For instance, Hu et al. [45] conducted a comparison of EEG classification for gender recognition using four entropy measures and six classifiers, concluding that fuzzy entropy combined with the boosting classifier yielded the most favorable results.

4.5. Evaluation of the Importance of Various Frequency Bands and Channels

The classification performance of spatial cognitive EEG signals is ranked from highest to lowest as follows: Gamma band, Beta2 band, Beta1 band, Delta band, Theta band, Alpha1 band, and Alpha2 band. This ranking of performance is consistent across various brain functional connectivity networks and their topological features. Furthermore, it aligns with findings from previous studies. For instance, Wen et al. [8,9] demonstrated that the combination of frequency bands, particularly Gamma and Beta2, exhibited the highest classification performance. The Gamma band is closely associated with complex cognitive functions, including memory, learning, and spatial cognition. Additionally, it plays a crucial role in the transmission and coordination of information across different brain regions. The Beta band, on the other hand, is linked to heightened activity in the cerebral cortex and is associated with advanced cognitive functions such as attention, reasoning, and decision-

making. Consequently, these two frequency bands are deemed most suitable for spatial cognitive EEG classification in VR games characterized by high levels of brain activity.

The selection of the Gamma frequency band was grounded in its well-documented association with higher-order cognitive functions, particularly spatial cognition, as well as its exceptional performance in classifying EEG signals before and after VR-based spatial cognitive training. An extensive analysis of other frequency bands further confirmed that the Gamma band provided the most discriminative features, underscoring its critical role in evaluating spatial cognitive training effects. The Gamma band is closely linked to advanced cognitive processes such as memory, attention, and spatial cognition, and it plays a pivotal role in integrating information across diverse brain regions—a capability essential for executing complex cognitive tasks. Empirical studies have consistently highlighted the significance of Gamma oscillations in tasks involving spatial memory and navigation, solidifying its suitability for analyzing spatial cognitive training outcomes. This comprehensive multi-band analysis not only ensures a thorough understanding of the underlying neural mechanisms, but also reinforces the robustness and reliability of the findings.

The contributions of EEG channels with left–right symmetric distribution to the classification of spatial cognitive signals are different. The most significant EEG channels for the classification of spatial cognitive EEG signals are Fp1, P8, and Cz. The Fp1 channel, situated in the frontal lobe, is associated with higher cognitive functions, including thinking, logic, memory, and planning, particularly those related to attention [47]. The P8 channel, located in the parietal lobe, is linked to cognitive functions such as perceptual integration, abstraction, and conceptualization, with a specific emphasis on short-term logical cognition. The Cz channel, positioned in the sensorimotor cortex at the midline of the brain, is related to somatosensory and motor functions and serves as the primary acquisition area for the Gamma band, which reflects the brain's short-term memory capabilities (i.e., immediate recall). Furthermore, the Cz channel acts as a convergence point for functional connections among various brain regions. Consequently, Fp1, P8, and Cz are identified as the three most critical channels for the classification of spatial cognitive EEG signals in the context of VR gaming. In summary, these EEG channels provide valuable insights into the neural mechanisms underlying spatial cognition. Monitoring their activity can help diagnose and understand spatial cognitive deficits in clinical populations, such as those with neurological disorders (e.g., stroke, Alzheimer's disease, or traumatic brain injury). Additionally, they can be used to evaluate the effectiveness of interventions aimed at improving spatial abilities.

4.6. Virtual Reality (VR) Game Features in Spatial Cognitive Outcomes

The effectiveness of the VR-based spatial cognitive training can be attributed to several key features of the game design, which were specifically tailored to stimulate spatial cognition.

The encoding and decoding tasks required participants to form and retrieve detailed mental maps of the racing tracks. This process strengthened spatial memory and navigation skills, as evidenced by the improved classification accuracy of post-training EEG signals. The inclusion of dynamic elements, such as moving obstacles and changing weather conditions, required participants to continuously update their spatial representations. This adaptive challenge enhanced participants' ability to process and respond to complex spatial information. Visual, auditory, and haptic cues helped participants maintain orientation and navigate the tracks more effectively. The multi-sensory feedback provided by the game reinforced spatial awareness and improved task performance. The progressive difficulty system ensured that participants were continuously challenged, promoting cognitive growth and skill development. This feature is particularly important for maintaining engagement and motivation over the course of the training program.

The findings of this study have important implications for the design of VR-based spatial cognitive training tools. Incorporating complex spatial tasks, such as encoding and decoding, can enhance spatial memory and navigation skills. Including dynamic elements in the game environment can promote adaptive spatial cognition and improve participants' ability to process complex spatial information. Providing multi-sensory feedback can reinforce spatial awareness and improve task performance. Implementing a progressive difficulty system can ensure continuous cognitive growth and skill development.

4.7. Limitations and Future Work

This study aligns with recent advancements in using network-derived features for cognitive performance classification, as demonstrated by Duma, Di Bono, and Mento (2021) [48], who showed that graph-theoretical measures of resting-state functional connectivity can predict cognitive control abilities. As opposed to this, we applied network topology features (e.g., degree, clustering coefficient, characteristic path length) to classify EEG signals before and after VR-based spatial cognitive training, achieving 97.82% accuracy in the Gamma band. While Duma et al. focused on resting-state EEG, our study used task-based EEG during VR training, suggesting that both approaches offer valuable insights into cognitive processes. Future research could integrate resting-state and task-based EEG to better understand cognitive training effects.

The study included 16 male participants due to logistical constraints and the need to control for gender-related variability in spatial cognition, despite documented gender differences in spatial task performance. Future work will expand to at least 60 participants, including both genders, diverse age groups, and cultural backgrounds, to enhance generalizability. Additionally, personalized VR training programs and long-term effects of VR training on spatial cognition should be explored, along with its applicability across cultural contexts.

The analysis focused on global and local network topological features (e.g., clustering coefficient, centrality) for EEG signal classification, omitting community structure metrics like modularity. Future studies will incorporate these to provide a more comprehensive understanding of neural mechanisms. Further directions include expanding VR game options for spatial cognitive training, developing a comprehensive EEG classification model for various VR tasks, and refining a convolutional neural network [49,50] model to extract spatiotemporal EEG features related to spatial cognition.

5. Conclusions

In this study, we present a novel framework for extracting topological features from spatial cognitive EEG networks using a cross fuzzy entropy network graph. The brain functional connectivity network is constructed using five distinct cross entropy measures. From the perspectives of global signal flow symmetry and local information aggregation, five types of network topological features are derived. The results demonstrate that cross fuzzy entropy is the most effective method for constructing brain functional connectivity networks. Among the extracted features, degree and clustering coefficient are identified as the top-performing local and global features, respectively, for classification tasks. Additionally, the Gamma frequency band is found to be the most effective for spatial cognitive EEG classification, with notable differences in the contributions of symmetrically distributed EEG channels on the left and right sides. Specifically, channels Fp1, P8, and Cz contribute the most to classification performance. The proposed model was validated on a spatial cognitive EEG dataset collected during VR gaming sessions, achieving a classification accuracy of 97.82%, outperforming existing models. These findings underscore that the cross fuzzy entropy-based approach for extracting topological features from brain functional

connectivity networks offers a highly interpretable and effective framework for evaluating spatial cognitive EEG.

While the proposed framework demonstrates promising results, this study has several limitations that can be improved in the future. First, the sample size used in this study is relatively small. Second, the sample consists exclusively of male participants. Third, the data were collected from a single institute. Future studies should aim to address these limitations by incorporating larger and more diverse datasets, including participants from different genders and multiple institutions, to validate and extend the findings of this work.

Author Contributions: Conceptualization, Y.Z. and H.L.; methodology, Y.Z. and X.L.; software, S.X. and X.L.; validation, Y.Z., S.X. and D.W.; formal analysis, S.X. and X.W.; investigation, Y.Z., X.L. and H.L.; resources, D.W. and X.W.; data curation, D.W.; writing—original draft preparation, Y.Z. and H.L.; writing—review and editing, Y.Z., S.X. and X.L.; visualization, S.X. and Y.Z.; supervision, H.L.; project administration, H.L.; funding acquisition, D.W. and X.W. All authors have read and agreed to the published version of the manuscript.

Funding: This research was funded by the [National Natural Science Foundation of China] [62276022, 62206014] from National Natural Science Foundation of China and the [National Key Research and Development Program of China] [2023YFF1203702, 2021YFF1200603] from Ministry of Science and Technology of China.

Institutional Review Board Statement: The study was conducted according to the guidelines of the Declaration of Helsinki, and approved by the Ethics Committee of University of Science and Technology Beijing (No. 2022-1-104).

Informed Consent Statement: Informed consent was obtained from all subjects involved in the study.

Data Availability Statement: All data generated or analyzed during this study are included in this published article. Derived data supporting the findings of this study are available from the corresponding author on request.

Conflicts of Interest: The authors declare no conflicts of interest.

References

1. Wen, D.; Yuan, J.; Li, J.; Sun, Y.; Wang, X.; Shi, R.; Wan, X.; Zhou, Y.; Song, H.; Dong, X.; et al. Design and Test of Spatial Cognitive Training and Evaluation System Based on Virtual Reality Head-Mounted Display with EEG Recording. *IEEE Trans. Neural Syst. Rehabil. Eng.* **2023**, *31*, 2705–2714. [CrossRef]
2. Johnson, E. A Study of the Effects of Immersion on Short-Term Spatial Memory. Master's Thesis, Purdue Polytechnic, West Lafayette, IN, USA, 2010.
3. Liao, Y.-Y.; Tseng, H.-Y.; Lin, Y.-J.; Wang, C.-J.; Hsu, W.-C. Using Virtual Reality-Based Training to Improve Cognitive Function, Instrumental Activities of Daily Living and Neural Efficiency in Older Adults with Mild Cognitive Impairment. *Eur. J. Phys. Rehabil. Med.* **2020**, *56*, 47–57. [CrossRef] [PubMed]
4. Allison, S.L.; Fagan, A.M.; Morris, J.C.; Head, D. Spatial Navigation in Preclinical Alzheimer's Disease. *J. Alzheimers Dis.* **2016**, *52*, 77–90. [CrossRef]
5. Kuliga, S.; von Stülpnagel, R.; Hölscher, C. Navigator-Driven Placement of Landmarks: Effects on Waynding Performance in a Virtual Tate Gallery. In *Cooperative Minds: Social Interaction and Group Dynamics, Proceedings of the 35th Annual Meeting of the Cognitive Science Society, Berlin, Germany, 31 July–3 August 2013*; Cognitive Science Society: Austin, TX, USA, 2013; p. 4012.
6. White, P.J.; Moussavi, Z. Neurocognitive Treatment for a Patient with Alzheimer's Disease Using a Virtual Reality Navigational Environment. *J. Exp. Neurosci.* **2016**, *10*, JEN-S40827. [CrossRef] [PubMed]
7. Cárdenas-Delgado, S.; Méndez-López, M.; Juan, M.; Pérez-Hernández, E.; Lluch, J.; Vivó, R. Using a Virtual Maze Task to Assess Spatial Short-Term Memory in Adults. In Proceedings of the 12th International Joint Conference on Computer Vision, Imaging and Computer Graphics Theory and Applications, Porto, Portugal, 27 February–1 March 2017; SCITEPRESS: Setubal, Portugal, 2017; pp. 46–57.
8. Wen, D.; Liang, B.; Li, J.; Wu, L.; Wan, X.; Dong, X.; Lan, X.; Song, H.; Zhou, Y. Feature Extraction Method of EEG Signals Evaluating Spatial Cognition of Community Elderly with Permutation Conditional Mutual Information Common Space Model. *IEEE Trans. Neural Syst. Rehabil. Eng.* **2023**, *31*, 2370–2380. [CrossRef]

9. Wen, D.; Li, R.; Jiang, M.; Li, J.; Liu, Y.; Dong, X.; Saripan, M.I.; Song, H.; Han, W.; Zhou, Y. Multi-Dimensional Conditional Mutual Information with Application on the EEG Signal Analysis for Spatial Cognitive Ability Evaluation. *Neural Netw.* **2022**, *148*, 23–36. [CrossRef] [PubMed]
10. Hadjiaros, M.; Neokleous, K.; Shimi, A.; Avraamides, M.N.N.; Pattichis, C.S.S. Virtual Reality Cognitive Gaming Based on Brain Computer Interfacing: A Narrative Review. *IEEE Access* **2023**, *11*, 18399–18416. [CrossRef]
11. Chiu, T.-C.; Gramann, K.; Ko, L.-W.; Duann, J.-R.; Jung, T.-P.; Lin, C.-T. Alpha Modulation in Parietal and Retrosplenial Cortex Correlates with Navigation Performance. *Psychophysiology* **2012**, *49*, 43–55. [CrossRef]
12. Lim, C.G.; Lee, T.S.; Guan, C.; Fung, D.S.S.; Zhao, Y.; Teng, S.S.W.; Zhang, H.; Krishnan, K.R.R. A Brain-Computer Interface Based Attention Training Program for Treating Attention Deficit Hyperactivity Disorder. *PLoS ONE* **2012**, *7*, e46692. [CrossRef] [PubMed]
13. Lin, C.-T.; Chiu, T.-C.; Gramann, K. EEG Correlates of Spatial Orientation in the Human Retrosplenial Complex. *NeuroImage* **2015**, *120*, 123–132. [CrossRef]
14. Drisdelle, B.L.; Aubin, S.; Jolicoeur, P. Dealing with Ocular Artifacts on Lateralized ERPs in Studies of Visual-Spatial Attention and Memory: ICA Correction versus Epoch Rejection. *Psychophysiology* **2017**, *54*, 83–99. [CrossRef]
15. Chouinard, S.; Brière, M.-È.; Rainville, C.; Godbout, R. Correlation between Evening and Morning Waking EEG and Spatial Orientation. *Brain Cogn.* **2003**, *53*, 162–165. [CrossRef]
16. Nishiyama, N.; Mizuhara, H.; Miwakeichi, F.; Yamaguchi, Y. Theta Episodes Observed in Human Scalp EEG during Virtual Navigation-Spatial Distribution and Task Dependence. In Proceedings of the 9th International Conference on Neural Information Processing, 2002, ICONIP'02, Singapore, 18–22 November 2002; IEEE: New York, NY, USA, 2002; Volume 1, pp. 428–432.
17. Li, X.; Yan, Y.; Wei, W. Identifying Patients with Poststroke Mild Cognitive Impairment by Pattern Recognition of Working Memory Load-Related ERP. *Comput. Math. Methods Med.* **2013**, *2013*, 658501. [CrossRef] [PubMed]
18. Pergher, V.; Wittevrongel, B.; Tournoy, J.; Schoenmakers, B.; Van Hulle, M.M. N-Back Training and Transfer Effects Revealed by Behavioral Responses and EEG. *Brain Behav.* **2018**, *8*, e01136. [CrossRef]
19. Baker, T.E.; Holroyd, C.B. The Topographical N170: Electrophysiological Evidence of a Neural Mechanism for Human Spatial Navigation. *Biol. Psychol.* **2013**, *94*, 90–105. [CrossRef]
20. Yang, K.; Hu, Y.; Zeng, Y.; Tong, L.; Gao, Y.; Pei, C.; Li, Z.; Yan, B. EEG Network Analysis of Depressive Emotion Interference Spatial Cognition Based on a Simulated Robotic Arm Docking Task. *Brain Sci.* **2024**, *14*, 44. [CrossRef] [PubMed]
21. Delorme, A.; Makeig, S. EEGLAB: An Open Source Toolbox for Analysis of Single-Trial EEG Dynamics Including Independent Component Analysis. *J. Neurosci. Methods* **2004**, *134*, 9–21. [CrossRef]
22. Chen, W.; Wang, Z.; Xie, H.; Yu, W. Characterization of Surface EMG Signal Based on Fuzzy Entropy. *IEEE Trans. Neural Syst. Rehabil. Eng.* **2007**, *15*, 266–272. [CrossRef]
23. Azami, H.; Li, P.; Arnold, S.E.; Escudero, J.; Humeau-Heurtier, A. Fuzzy Entropy Metrics for the Analysis of Biomedical Signals: Assessment and Comparison. *IEEE Access* **2019**, *7*, 104833–104847. [CrossRef]
24. Xie, H.-B.; Zheng, Y.-P.; Guo, J.-Y.; Chen, X. Cross-Fuzzy Entropy: A New Method to Test Pattern Synchrony of Bivariate Time Series. *Inf. Sci.* **2010**, *180*, 1715–1724. [CrossRef]
25. Flood, M.W.; Grimm, B. EntropyHub: An Open-Source Toolkit for Entropic Time Series Analysis. *PLoS ONE* **2021**, *16*, e0259448. [CrossRef] [PubMed]
26. Ismail, L.E.; Karwowski, W. A Graph Theory-Based Modeling of Functional Brain Connectivity Based on EEG: A Systematic Review in the Context of Neuroergonomics. *IEEE Access* **2020**, *8*, 155103–155135. [CrossRef]
27. Hagberg, A.; Swart, P.J.; Schult, D.A. *Exploring Network Structure, Dynamics, and Function Using NetworkX*; Los Alamos National Laboratory (LANL): Los Alamos, NM, USA, 2008.
28. Costantini, G.; Perugini, M. Generalization of Clustering Coefficients to Signed Correlation Networks. *PLoS ONE* **2014**, *9*, e88669. [CrossRef] [PubMed]
29. Fagiolo, G. Clustering in Complex Directed Networks. *Phys. Rev. E* **2007**, *76*, 026107. [CrossRef] [PubMed]
30. Qi, X.; Fuller, E.; Wu, Q.; Wu, Y.; Zhang, C.-Q. Laplacian Centrality: A New Centrality Measure for Weighted Networks. *Inf. Sci.* **2012**, *194*, 240–253. [CrossRef]
31. Chen, T.; Guestrin, C. XGBoost: A Scalable Tree Boosting System. In Proceedings of the 22nd ACM SIGKDD International Conference on Knowledge Discovery and Data Mining, San Francisco, CA, USA, 13–17 August 2016; ACM: New York, NY, USA, 2016; pp. 785–794.
32. Lotte, F.; Guan, C. Regularizing Common Spatial Patterns to Improve BCI Designs: Unified Theory and New Algorithms. *IEEE Trans. Biomed. Eng.* **2010**, *58*, 355–362. [CrossRef]
33. Bashashati, A.; Fatourechi, M.; Ward, R.K.; Birch, G.E. A Survey of Signal Processing Algorithms in Brain–Computer Interfaces Based on Electrical Brain Signals. *J. Neural Eng.* **2007**, *4*, R32. [CrossRef]
34. Alvarado-Gonzalez, M.; Fuentes-Pineda, G.; Cervantes-Ojeda, J. A Few Filters Are Enough: Convolutional Neural Network for P300 Detection. *Neurocomputing* **2021**, *425*, 37–52. [CrossRef]

35. Li, M.; Li, J.; Zheng, X.; Ge, J.; Xu, G. MSHANet: A Multi-Scale Residual Network with Hybrid Attention for Motor Imagery EEG Decoding. *Cogn. Neurodyn.* **2024**, *18*, 3463–3476. [CrossRef]
36. Lawhern, V.J.; Solon, A.J.; Waytowich, N.R.; Gordon, S.M.; Hung, C.P.; Lance, B.J. EEGNet: A Compact Convolutional Neural Network for EEG-Based Brain–Computer Interfaces. *J. Neural Eng.* **2018**, *15*, 056013. [CrossRef]
37. Nunez, P.L.; Srinivasan, R.; Westdorp, A.F.; Wijesinghe, R.S.; Tucker, D.M.; Silberstein, R.B.; Cadusch, P.J. EEG Coherency: I: Statistics, Reference Electrode, Volume Conduction, Laplacians, Cortical Imaging, and Interpretation at Multiple Scales. *Electroencephalogr. Clin. Neurophysiol.* **1997**, *103*, 499–515. [CrossRef]
38. Lachaux, J.-P.; Rodriguez, E.; Martinerie, J.; Varela, F.J. Measuring Phase Synchrony in Brain Signals. *Hum. Brain Mapp.* **1999**, *8*, 194–208. [CrossRef]
39. Vinck, M.; Oostenveld, R.; Van Wingerden, M.; Battaglia, F.; Pennartz, C.M. An Improved Index of Phase-Synchronization for Electrophysiological Data in the Presence of Volume-Conduction, Noise and Sample-Size Bias. *Neuroimage* **2011**, *55*, 1548–1565. [CrossRef] [PubMed]
40. Nolte, G.; Bai, O.; Wheaton, L.; Mari, Z.; Vorbach, S.; Hallett, M. Identifying True Brain Interaction from EEG Data Using the Imaginary Part of Coherency. *Clin. Neurophysiol.* **2004**, *115*, 2292–2307. [CrossRef] [PubMed]
41. Lundberg, S.M.; Erion, G.G.; Lee, S.-I. Consistent Individualized Feature Attribution for Tree Ensembles. *arXiv* **2018**, arXiv:1802.03888.
42. Stefano Filho, C.A.; Attux, R.; Castellano, G. Can Graph Metrics Be Used for EEG-BCIs Based on Hand Motor Imagery? *Biomed. Signal Process. Control* **2018**, *40*, 359–365. [CrossRef]
43. Tibdewal, M.N.; Dey, H.R.; Mahadevappa, M.; Ray, A.; Malokar, M. Multiple Entropies Performance Measure for Detection and Localization of Multi-Channel Epileptic EEG. *Biomed. Signal Process. Control* **2017**, *38*, 158–167. [CrossRef]
44. Xiang, J.; Li, C.; Li, H.; Cao, R.; Wang, B.; Han, X.; Chen, J. The Detection of Epileptic Seizure Signals Based on Fuzzy Entropy. *J. Neurosci. Methods* **2015**, *243*, 18–25. [CrossRef] [PubMed]
45. Hu, J. An Approach to EEG-Based Gender Recognition Using Entropy Measurement Methods. *Knowl.-Based Syst.* **2018**, *140*, 134–141. [CrossRef]
46. Corsi, M.-C.; Troisi Lopez, E.; Sorrentino, P.; Cuozzo, S.; Danieli, A.; Bonanni, P.; Duma, G.M. Neuronal Avalanches in Temporal Lobe Epilepsy as a Noninvasive Diagnostic Tool Investigating Large Scale Brain Dynamics. *Sci. Rep.* **2024**, *14*, 14039. [CrossRef]
47. Albright, T.D.; Kandel, E.R.; Posner, M.I. Cognitive Neuroscience. *Curr. Opin. Neurobiol.* **2000**, *10*, 612–624. [CrossRef] [PubMed]
48. Duma, G.M.; Di Bono, M.G.; Mento, G. Grounding Adaptive Cognitive Control in the Intrinsic, Functional Brain Organization: An HD-EEG Resting State Investigation. *Brain Sci.* **2021**, *11*, 1513. [CrossRef]
49. Chauhan, S.; Vashishtha, G.; Zimroz, R.; Kumar, R.; Gupta, M.K. Optimal Filter Design Using Mountain Gazelle Optimizer Driven by Novel Sparsity Index and Its Application to Fault Diagnosis. *Appl. Acoust.* **2024**, *225*, 110200. [CrossRef]
50. Vashishtha, G.; Chauhan, S.; Sehri, M.; Hebda-Sobkowicz, J.; Zimroz, R.; Dumond, P.; Kumar, R. Advancing Machine Fault Diagnosis: A Detailed Examination of Convolutional Neural Networks. *Meas. Sci. Technol.* **2025**, *36*, 022001. [CrossRef]

Disclaimer/Publisher's Note: The statements, opinions and data contained in all publications are solely those of the individual author(s) and contributor(s) and not of MDPI and/or the editor(s). MDPI and/or the editor(s) disclaim responsibility for any injury to people or property resulting from any ideas, methods, instructions or products referred to in the content.